Available online at www.sciencedirect.com
SCIENCE DIRECT®
ELSEVIER
International Journal of Solids and Structures 43 (2006) 3832–3855
INTERNATIONAL JOURNAL OF SOLIDS and STRUCTURES
www.elsevier.com/locate/ijsolstr

Eigenanalysis and continuum modelling of pre-twisted repetitive beam-like structures

N.G. Stephen *, Y. Zhang

School of Engineering Sciences, Mechanical Engineering, University of Southampton, Highfield, Southampton SO17 1BJ, UK

Received 19 May 2005
Available online 11 July 2005

Abstract

A repetitive pin-jointed, pre-twisted structure is analysed using a state variable transfer matrix technique. Within a global coordinate system the transfer matrix is periodic, but introduction of a local coordinate system rotating with nodal cross-sections results in an autonomous transfer matrix for this Floquet system. Eigenanalysis reveals four real unity eigenvalues, indicating tension–torsion coupling, and equivalent continuum properties such as Poisson's ratio, cross-sectional area, torsion constant and the tension–torsion coupling coefficient are determined. A variety of real and complex near diagonal Jordan decompositions are possible for the multiple (eight) complex unity eigenvalues and these are discussed in some detail. Analysis of the associated principal vectors shows that a bending moment produces curvature in the plane of the moment, together with shear deformation in the perpendicular plane, but no bending–bending coupling; the choice of a structure having an equilateral triangular cross-section is thought responsible for this unexpected behaviour, as the equivalent continuum second moments of area are equal about all cross-sectional axes. In addition, an asymmetric stiffness matrix is obtained for bending moment and shearing force coupling, and possible causes are discussed.

Keywords: Pre-twist; Repetitive; Floquet; Jordan canonical forms; Eigenproblem; Tension–torsion; Bending–shear; Continuum; Homogenisation; Properties

1. Introduction

Repetitive (or periodic) structures are analysed most efficiently when that periodicity is taken into account. It is possible to determine the behaviour of the complete structure from analysis of a single repeating

* Corresponding author. Tel.: +44 (0) 23 80592359; fax: +44 (0) 23 80593230.
E-mail address: ngs@soton.ac.uk (N.G. Stephen).

0020-7683/$ - see front matter © 2005 Elsevier Ltd. All rights reserved.
doi:10.1016/j.ijsolstr.2005.05.023

Nomenclature

A	cross-sectional area
d	member diameter
$\mathbf{d}$	nodal displacement vector
E	Young's modulus
$\mathbf{F}$	force vector
G, $\mathbf{G}$	shear modulus, transfer matrix
H	height of cell cross-section ($H = \sqrt{3}L/2$)
i, I, $\mathbf{I}$	$\sqrt{-1}$, second moment of area, identity matrix
J, $\mathbf{J}$, $\mathbf{J}_{\mathrm{m}}$	torsion constant, Jordan block and canonical form, metric
$\mathbf{K}$, K	stiffness matrix, coupling coefficient
L	length of cell, and of cross-sectional members, left
M	bending or twisting moment
n, N, $\mathbf{N}$	index of cell or section, compliance matrix
p	period
Q	shearing force
R	radius of bending curvature, right
$\mathbf{s}$	state vector
T	tensile force
$\mathbf{T}$	orthogonal coordinate transformation matrix
u, v, w	displacements in the x-, y- and z-directions
$\mathbf{v}$	eigenvector
$\mathbf{V}$	similarity/transformation matrix of eigen- and principal (generalised) vectors
$\mathbf{w}$	principal vector
x, y, z	global Cartesian coordinate system at the zeroth nodal location
α	pre-twist angle per cell
γ	shear angle
ε	direct strain
θ	(torsional) rotation about the x-axis
κ	shear coefficient
λ	decay factor, eigenvalue
ν	Poisson's ratio
ψ	cross-sectional rotation

cell, together with knowledge of the boundary conditions. Straight (prismatic) repetitive one-dimensional (beam-like) structures have previously been analysed by Stephen and Wang (1996) as an eigenproblem for a state vector transfer matrix. The state vectors $\mathbf{s}_{\mathrm{L}}$ and $\mathbf{s}_{\mathrm{R}}$ consist of the nodal displacement and force components on the left- and right-hand sides, respectively, of the single cell of the repetitive structure, while the transfer matrix $\mathbf{G}$ is obtained through manipulation of the single cell stiffness matrix, $\mathbf{K}$. Non-unity eigenvalues of $\mathbf{G}$ occur as reciprocals, and describe the rate of decay of self-equilibrated end loading, as anticipated by Saint-Venant's principle. Multiple unity eigenvalues pertain to the transmission modes of tension, torsion, bending moment and shear, together with the rigid body displacements and rotations. From knowledge of the eigen- and principal vectors associated with the unity eigenvalues, equivalent continuum beam properties of cross-sectional area, Poisson's ratio, second moment of area, torsion constant and shear coefficient were calculated. The present paper extends this approach to pin-jointed structures

having a pre-twisted form. Each cell has a constant angle of pre-twist, taken to be an integer fraction of 2π, so that one has a spatial, rather than the more usual temporal, periodic Floquet system.

For continuum structures, pre-twist produces tension–torsion and bending–bending couplings, and has been studied widely (see the review by Rosen (1991) citing over 200 references) because of the importance of the engineering applications, ranging from turbine blades and propellers, to architectural columns. It is easy to visualise that a pre-twisted beam will increase in length if a twisting moment is applied in a direction tending to decrease the pre-twist angle; equivalently, a tensile force will produce both an extension and a reduction in pre-twist angle. Bending–bending coupling is not so easy to visualise: consider a straight beam, such as a metal ruler, for which the bending stiffness' in the two principal planes are quite unequal; if subject to excessive compressive load, buckling would favour deflection in the flexible plane. Suppose, now, that this beam has a total uniform pre-twist through 90°, and that a bending moment is applied at one end (left-hand, say) in the flexible plane *at that end*; at the right-hand end, the moment is in the stiff plane. Thus at the two ends, there would be curvature in just one plane; bending deflection would again favour the flexible plane, and be much greater at the left-hand end. The above is easy to visualise: less so, is the behaviour at locations between the two ends. If there is a coupled bending curvature perpendicular to that of the applied bending moment, then clearly its magnitude must vary from zero to zero over the 90° twist of the beam; in turn, there are two obvious possibilities: either that it depends on double the pre-twist angle in a sinusoidal form, or that it remains zero throughout. Existing theories are based on the former; however the example pre-twisted structure considered in the present paper does not exhibit such bending–bending coupling, presumably because the chosen equilateral triangular cross-section has equal equivalent continuum second moments of area about all cross-sectional axes. On the other hand, the example structure does exhibit a bending-shear coupling, which is not included in the majority of such theories.

Previous research on continuum pre-twisted structures may be classified as within the spirit of *Strength of Materials*, or the more exact three-dimensional *Theory of Elasticity*. The former is based largely upon the so-called *helical fibre assumption* first introduced by Chen (1951),[1] in which the longitudinal stress in the bar cross-section is not parallel to the axis, but acts in the direction of the longitudinal spiral fibres of the pre-twisted bar. The typical approach of the latter, see for example Okubo (1951, 1953, 1954), Goodier and Griffin (1969), Shield (1982), Krenk (1983a,b), Pucci and Risitano (1996) and Guglielmino and Saccomandi (1996), is the introduction of a local coordinate system, which rotates with the principal axes of the cross-section, into the governing differential equations for stress describing force equilibrium, or the equivalent (Navier) equations for displacements; while the equilibrium equations become more complicated, the advantage is that the traction-free boundary condition becomes independent of the axial coordinate. In the present work, the introduction of a local coordinate system rotating with the cross-section leads to a transfer matrix which is autonomous, that is, independent of location; one now has translational symmetry, allowing eigenanalysis.

The paper is laid out as follows: in Section 2, we describe the example structure; a pin-jointed framework was chosen so that predictions from the present approach could be verified by comparison with exact finite element analysis (FEA). In Section 3, the transfer matrix approach is outlined for a straight structure, the necessary modifications for a pre-twisted structure and the relationship with Floquet theory are noted. Coordinate transformations leading to the autonomous transfer matrix are developed, and its symplectic properties noted. In Section 4, eigenanalysis of the autonomous transfer matrix is performed, and the variety of possible real and complex Jordan block decompositions introduced and discussed; apart from some example-specific decay eigenvalues, the analysis is applicable to any repetitive pre-twisted structure. Section 5 describes the coupling of eigen- and principal vectors according to the real Jordan block forms, from which the example-specific equivalent continuum beam properties are determined. Conclusions are drawn

[1] In the literature, Chen Chu is most often referred to according to his given name, Chu.

in Section 6, and the transformation matrix leading to the real Jordan block form, and modified shear vectors are presented in Appendices A and B.

2. Example structure

We consider a pin-jointed beam-like framework whose cross-section is in the form of an equilateral triangle of side length $L = 0.3428$ m. The zeroth nodal cross-section is assumed to align with a global $x\ y\ z$ coordinate system (x is the axial direction), Fig. 1(a), while the adjacent $n = 1$ nodal cross-section, Fig. 1(b), is pre-twisted through angle α radians, here taken as $\alpha = \pi/8$; also shown is a local coordinate system $x'\ y'\ z'$ which rotates with the cross-section. The axial length of the cell is also taken to be $L = 0.3428$ m. Individual members of the cell are of aluminium, having Young's modulus $E = 70 \times 10^9$ N/m^2 and diameter $d = 6.35$ mm. The longitudinal (helical) members, together with the two diagonals in each external face of the cell, have length as demanded by the relevant nodal locations, that is, the pre-twisted structure is free of any pre-load. The complete first cell of the framework, Fig. 2, is shown in bold.

3. Transfer matrix

For a straight repetitive structure, the stiffness matrix $\mathbf{K}$ for a typical cell is first constructed employing the global coordinate system which is, of course, applicable to all cells; cross-sectional members are regarded as being shared by adjacent cells, so are treated as having one-half of their actual stiffness. The stiffness matrix relates nodal force and displacement components as

$$\begin{bmatrix} \mathbf{F}_\mathrm{L} \\ \mathbf{F}_\mathrm{R} \end{bmatrix} = \begin{bmatrix} \mathbf{K}_{\mathrm{LL}} & \mathbf{K}_{\mathrm{LR}} \\ \mathbf{K}_{\mathrm{RL}} & \mathbf{K}_{\mathrm{RR}} \end{bmatrix} \begin{bmatrix} \mathbf{d}_\mathrm{L} \\ \mathbf{d}_\mathrm{R} \end{bmatrix} \tag{1}$$

the transfer matrix $\mathbf{G}$, in global coordinates, is then calculated as

$$\begin{bmatrix} \mathbf{d}_\mathrm{R} \\ \mathbf{F}_\mathrm{R} \end{bmatrix} = \begin{bmatrix} -\mathbf{K}_{\mathrm{LR}}^{-1}\mathbf{K}_{\mathrm{LL}} & -\mathbf{K}_{\mathrm{LR}}^{-1} \\ \mathbf{K}_{\mathrm{RL}} - \mathbf{K}_{\mathrm{RR}}\mathbf{K}_{\mathrm{LR}}^{-1}\mathbf{K}_{\mathrm{LL}} & -\mathbf{K}_{\mathrm{RR}}\mathbf{K}_{\mathrm{LR}}^{-1} \end{bmatrix} \begin{bmatrix} \mathbf{d}_\mathrm{L} \\ -\mathbf{F}_\mathrm{L} \end{bmatrix}, \tag{2}$$

or, more compactly

$$\mathbf{s}_\mathrm{R} = \mathbf{G}\mathbf{s}_\mathrm{L}, \tag{3}$$

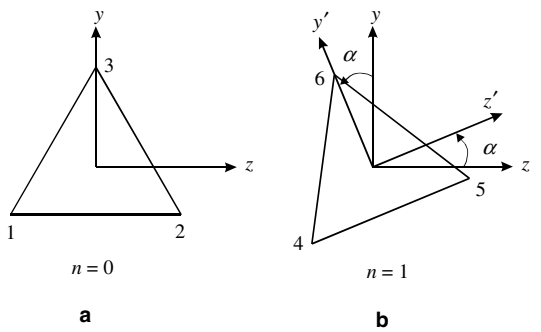

Fig. 1. Local and global coordinate systems on the left- and right-hand side of the first cell, respectively.

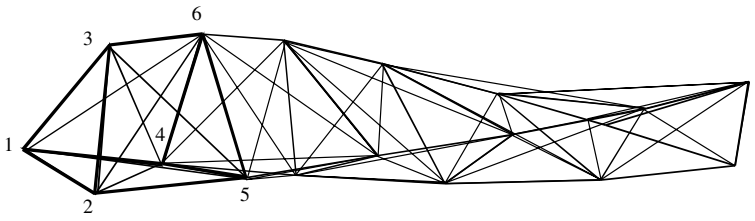

Fig. 2. A six cell pin-jointed pre-twisted framework; the first cell is shown in bold.

where the state vectors, and the transfer matrix $\mathbf{G}$, are defined accordingly. In the above, the subscripts L and R are employed to denote left- and right-hand sides of the cell, while $\mathbf{G}$ is the same for all cells; the force vector within $\mathbf{s}_{\mathrm{L}}$ requires a minus sign, as the state vectors are defined according to the conventions of the Theory of Elasticity, rather than FEA. The above is an adequate description for the straight structure, which possesses translational symmetry, but is inadequate for the pre-twisted structure for which, in global coordinates, the transfer matrix for each cell within a cycle is different. Instead we write for the first cell, Fig. 2,

$$\mathbf{s}(1) = \mathbf{G}(1)\mathbf{s}(0), \tag{4}$$

and for the typical nth cell

$$\mathbf{s}(n) = \mathbf{G}(n)\mathbf{s}(n-1), \tag{5}$$

where the state vector subscript has been replaced by an argument, to denote the nodal location, and the transfer matrix $\mathbf{G}$ requires an index to identify the cell.

Assuming that the pre-twist angle α for each cell is constant, then the transfer matrix $\mathbf{G}(n)$ is periodic, with period $p = 2\pi/\alpha$, that is

$$\mathbf{G}(n+p) = \mathbf{G}(n), \tag{6}$$

and for the present example $p = 16$. For simplicity, suppose that the Nth nodal cross-section aligns with the global coordinate system; so too will the $(N+p)$th. Suppose that one constructs a stiffness matrix for all p cells, and then condense this to form a super-element stiffness matrix $\mathbf{K}_p$ relating force and displacement components on the Nth and the $(N+p)$th nodal locations. Note that the subscript p has been employed to denote a complete cycle of p cells. From this, one could construct a transfer matrix $\mathbf{G}_p$, using Eq. (2), which is known as the monodromy matrix; note that $\mathbf{G}_p = \Pi_{n=1}^{p}\mathbf{G}(n)$. One could then perform eigenanalysis in the usual way; that is, denoting the state vectors as $\mathbf{s}_p(N)$ and $\mathbf{s}_p(N+p)$, respectively, gives

$$\mathbf{s}_p(N+p) = \mathbf{G}_p\mathbf{s}_p(N) \quad \text{and} \quad \mathbf{s}_p(N+p) = \lambda_p\mathbf{s}_p(N) \tag{7}$$

to give the eigenproblem

$$(\mathbf{G}_p - \lambda_p\mathbf{I})\mathbf{s}_p(N) = 0. \tag{8}$$

Denote the square matrix comprised of the eigen- and principal vectors of the above as $\mathbf{V}_p(N)$; this transforms the transfer matrix to the Jordan canonical form $\mathbf{J}_p$, according to

$$\mathbf{V}_p(N)^{-1}\mathbf{G}_p\mathbf{V}_p(N) = \mathbf{J}_p. \tag{9}$$

The process described above allows one to treat the pre-twisted beam as if it were straight; however, state vectors are only defined at those cross-sections that align with the global coordinate system, and

the information contained within the eigen- and principal vectors describes the behaviour of a complete cycle of p cells. Such a procedure is exactly how periodic systems are often treated using Floquet theory; see, for example, Kelley and Peterson (2001). The eigenvalues λ_p are known as Floquet multipliers, and define the stability of a (usually dynamic) periodic system which most often is all that is required.

Instead, introduce an autonomous transfer matrix $\mathbf{G}'$, which is independent of the cell index, n, by employing a local coordinate system; refer to Fig. 1 for the first cell, and note that the left-hand side aligns with the global x y z coordinate system. The local right-hand side nodal coordinates transform as

$$\begin{bmatrix} x' \\ y' \\ z' \end{bmatrix} = \begin{bmatrix} 1 & 0 & 0 \\ 0 & \cos\alpha & \sin\alpha \\ 0 & -\sin\alpha & \cos\alpha \end{bmatrix} \begin{bmatrix} x \\ y \\ z \end{bmatrix} = \mathbf{T}_3 \begin{bmatrix} x \\ y \\ z \end{bmatrix}, \tag{10}$$

where the 3×3 orthogonal transformation matrix $\mathbf{T}_3$ is defined accordingly. On the other hand, nodal displacement and force components, referring to node 4 in Fig. 1(b), transform as

$$\begin{bmatrix} F'_{4x} \\ F'_{4y} \\ F'_{4z} \end{bmatrix} = \begin{bmatrix} 1 & 0 & 0 \\ 0 & \cos\alpha & -\sin\alpha \\ 0 & \sin\alpha & \cos\alpha \end{bmatrix} \begin{bmatrix} F_{4x} \\ F_{4y} \\ F_{4z} \end{bmatrix} = \mathbf{T}_3^{\mathrm{T}} \begin{bmatrix} F_{4x} \\ F_{4y} \\ F_{4z} \end{bmatrix} \tag{11}$$

and

$$\begin{bmatrix} d'_{4x} \\ d'_{4y} \\ d'_{4z} \end{bmatrix} = \begin{bmatrix} 1 & 0 & 0 \\ 0 & \cos\alpha & -\sin\alpha \\ 0 & \sin\alpha & \cos\alpha \end{bmatrix} \begin{bmatrix} d_{4x} \\ d_{4y} \\ d_{4z} \end{bmatrix} = \mathbf{T}_3^{\mathrm{T}} \begin{bmatrix} d_{4x} \\ d_{4y} \\ d_{4z} \end{bmatrix}. \tag{12}$$

Extending this scheme to the other nodes, the state vector on the right-hand side may be written in the local coordinate system as

$$\mathbf{s}'(1) = \mathbf{T}_{18}^{\mathrm{T}} \mathbf{s}(1), \tag{13}$$

where $\mathbf{T}_{18}^{\mathrm{T}}$ is the 18×18 transformation matrix consisting of $\mathbf{T}_3^{\mathrm{T}}$ blocks on the leading diagonal, but zero elsewhere. Now pre-multiply Eq. (4) by $\mathbf{T}_{18}^{\mathrm{T}}$ to give

$$\mathbf{T}_{18}^{\mathrm{T}} \mathbf{s}(1) = \mathbf{T}_{18}^{\mathrm{T}} \mathbf{G}(1) \mathbf{s}(0), \quad \text{or } \mathbf{s}'(1) = \mathbf{G}' \mathbf{s}(0), \tag{14}$$

where

$$\mathbf{G}' = \mathbf{T}_{18}^{\mathrm{T}} \mathbf{G}(1). \tag{15}$$

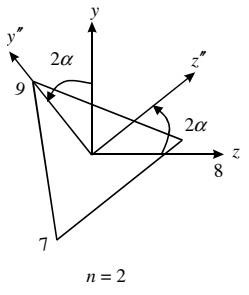

Fig. 3. Coordinates of the right-hand side of the second cell.

Each cell within the cycle requires a transformation matrix to relate the local coordinate system with the global, although this is not required for the eigenanalysis; the pattern is easily discerned by considering the second cell, Fig. 3, (where a double prime notation is temporarily, and somewhat unsatisfactorily, employed) whose local right-hand side coordinates transform as

$$\begin{bmatrix} x'' \\ y'' \\ z'' \end{bmatrix} = \begin{bmatrix} 1 & 0 & 0 \\ 0 & \cos\alpha & \sin\alpha \\ 0 & -\sin\alpha & \cos\alpha \end{bmatrix} \begin{bmatrix} x' \\ y' \\ z' \end{bmatrix} = \begin{bmatrix} 1 & 0 & 0 \\ 0 & \cos\alpha & \sin\alpha \\ 0 & -\sin\alpha & \cos\alpha \end{bmatrix}^2 \begin{bmatrix} x \\ y \\ z \end{bmatrix} = \begin{bmatrix} 1 & 0 & 0 \\ 0 & \cos 2\alpha & \sin 2\alpha \\ 0 & -\sin 2\alpha & \cos 2\alpha \end{bmatrix} \begin{bmatrix} x \\ y \\ z \end{bmatrix}$$
$$= \mathbf{T}_3(2) \begin{bmatrix} x \\ y \\ z \end{bmatrix}, \tag{16}$$

where the index 2 denotes a rotation by angle 2α, and the transformation matrix for the first cell strictly requires index 1. Suppose that the transfer matrix for this second cell had been calculated in global coordinates according to $\mathbf{s}(2) = \mathbf{G}(2)\mathbf{s}(1)$. In the local coordinates *for this cell*, one has $\mathbf{s}'(2) = \mathbf{T}_{18}^{\mathrm{T}}(2)\mathbf{s}(2)$, and $\mathbf{s}'(1) = \mathbf{T}_{18}^{\mathrm{T}}(1)\mathbf{s}(1)$, or $\mathbf{s}(1) = \mathbf{T}_{18}(1)\mathbf{s}'(1)$, since the transformation matrix is orthogonal. Pre-multiply by $\mathbf{T}_{18}^{\mathrm{T}}(2)$ in the above to give $\mathbf{T}_{18}^{\mathrm{T}}(2)\mathbf{s}(2) = \mathbf{T}_{18}^{\mathrm{T}}(2)\mathbf{G}(2)\mathbf{s}(1)$ or $\mathbf{s}'(2) = \mathbf{G}'(2)\mathbf{s}'(1)$ where $\mathbf{G}'(2) = \mathbf{T}_{18}^{\mathrm{T}}(2)\mathbf{G}(2)\mathbf{T}_{18}(1)$.

For the nth cell, one has in global coordinates $\mathbf{s}(n) = \mathbf{G}(n)\mathbf{s}(n-1)$; in local coordinates $\mathbf{s}'(n) = \mathbf{T}_{18}^{\mathrm{T}}(n)\mathbf{s}(n)$, $\mathbf{s}(n-1) = \mathbf{T}_{18}(n-1)\mathbf{s}'(n-1)$. Pre-multiply by $\mathbf{T}_{18}^{\mathrm{T}}(n)$ in the above to give $\mathbf{T}_{18}^{\mathrm{T}}(n)\mathbf{s}(n) = \mathbf{T}_{18}^{\mathrm{T}}(n)\mathbf{G}(n)\mathbf{s}(n-1)$ or $\mathbf{s}'(n) = \mathbf{G}'(n)\mathbf{s}'(n-1)$ so the transformation for the general cell is

$$\mathbf{G}'(n) = \mathbf{T}_{18}^{\mathrm{T}}(n)\mathbf{G}(n)\mathbf{T}_{18}(n-1); \tag{17}$$

note that for the first cell, this reduces to Eq. (15) as $\mathbf{T}_{18}(0)$ is the identity matrix.

Expressed within the local coordinates of the cell under consideration, the transfer matrix is invariant; that is

$$\mathbf{G}' = \mathbf{G}'(1) = \cdots = \mathbf{G}'(n) \cdots = \mathbf{G}'(p). \tag{18}$$

The transfer matrix $\mathbf{G}'$ has the property of being symplectic, as does $\mathbf{G}(1)$; each satisfies the relationship $\mathbf{G}^{\mathrm{T}}\mathbf{J}_{\mathrm{m}}\mathbf{G} = \mathbf{J}_{\mathrm{m}}$, where $\mathbf{J}_{\mathrm{m}}$ is the metric matrix $\mathbf{J}_{\mathrm{m}} = \begin{bmatrix} \mathbf{0} & \mathbf{I} \\ -\mathbf{I} & \mathbf{0} \end{bmatrix}$, $\mathbf{I}$ is the identity matrix of the appropriate size, and $\mathbf{J}_{\mathrm{m}}^{\mathrm{T}} = \mathbf{J}_{\mathrm{m}}^{-1} = -\mathbf{J}_{\mathrm{m}}$. For $\mathbf{G}(1)$, this can be proven by direct substitution from Eq. (2), and noting that the stiffness matrix $\mathbf{K}$ is symmetric. For $\mathbf{G}'$, start from the relationship $\mathbf{G}(1)^{\mathrm{T}}\mathbf{J}_{\mathrm{m}}\mathbf{G}(1) = \mathbf{J}_{\mathrm{m}}$, and substitute from Eq. (15) to give $\mathbf{G}'^{\mathrm{T}}\mathbf{T}_{18}^{\mathrm{T}}\mathbf{J}_{\mathrm{m}}\mathbf{T}_{18}\mathbf{G}' = \mathbf{J}_{\mathrm{m}}$; last, partition the transformation matrix as $\mathbf{T}_{18} = \begin{bmatrix} \mathbf{T}_9 & \mathbf{0} \\ \mathbf{0} & \mathbf{T}_9 \end{bmatrix}$, and expand to find that $\mathbf{T}_{18}^{\mathrm{T}}\mathbf{J}_{\mathrm{m}}\mathbf{T}_{18}$ is equal to $\mathbf{J}_{\mathrm{m}}$, noting that the transpose of $\mathbf{T}_9$ is equal to its inverse.

4. Eigenanalysis

Since the structure, using the local coordinate system, now possesses translational symmetry, two consecutive state vectors are related by the scalar λ as

$$\mathbf{s}'(n+1) = \lambda\mathbf{s}'(n), \tag{19}$$

which, together with the transfer matrix relation, $\mathbf{s}'(n+1) = \mathbf{G}'\mathbf{s}'(n)$, immediately leads to the eigenvalue problem

$$\mathbf{G}'\mathbf{s}'(n) = \lambda\mathbf{s}'(n). \tag{20}$$

Although the transfer matrix $\mathbf{G}'$ is identical for all cells, we specifically consider the first cell, for which the left-hand cross-section aligns with the global coordinate system; this facilitates interpretation of the eigen- and principal vectors.

The *eig* command within MATLAB gives the eigenvalues of the transfer matrix $\mathbf{G}'$ as the three reciprocal pairs

$$\begin{bmatrix}\lambda_1 = -22.3303\\ \lambda_1^{-1} = -0.0488\end{bmatrix},\quad \begin{bmatrix}\lambda_2 = -10.0110(1+\mathrm{i})\\ \lambda_2^{-1} = -0.0499(1-\mathrm{i})\end{bmatrix},\quad \begin{bmatrix}\bar{\lambda}_2 = -10.0110(1-\mathrm{i})\\ \bar{\lambda}_2^{-1} = -0.0499(1+\mathrm{i})\end{bmatrix}, \tag{21}$$

which describe decay of self-equilibrated loading, and four real unity eigenvalues pertaining to rigid body displacement in, and rigid body rotation about, the x-direction, together with tension and torsion. Also there are eight complex unity eigenvalues of the form $4\times \mathrm{e}^{\pm \mathrm{i}\alpha}$, in which α is the angle of pre-twist per cell, and these relate to rigid body displacements in, and rigid body rotations about, both the y- and z-directions, together with bending moments and shearing forces in both planes.

As with the eigenanalysis described by Stephen and Wang (1996), the eigenvectors associated with the distinct decay eigenvalues are correctly calculated by the QR algorithm employed within MATLAB, and these are designated $\mathbf{v}_1$ to $\mathbf{v}_6$. On the other hand, the eigenvectors describing rigid body displacements in the x-direction, $\mathbf{v}_7$, and rotation about the x-axis, $\mathbf{v}_9$, are determined from the reduced row echelon form (*rref*) of $(\mathbf{G}'-\mathbf{I})$, and may be written as

$$\mathbf{v}_7 = [1\ \ 0\ \ 0\ \ 1\ \ 0\ \ 0\ \ 1\ \ 0\ \ 0\ \ 0\ \ 0\ \ 0\ \ 0\ \ 0\ \ 0\ \ 0\ \ 0\ \ 0]^{\mathrm{T}}\times 10^{-8}, \tag{22}$$

$$\mathbf{v}_9 = [0\ \ L\theta/2\ \ -H\theta/3\ \ 0\ \ -L\theta/2\ \ -H\theta/3\ \ 0\ \ 0\ \ 2H\theta/3\ \ 0\ \ 0\ \ 0\ \ 0\ \ 0\ \ 0\ \ 0\ \ 0\ \ 0]^{\mathrm{T}}, \tag{23}$$

where the angle of rotation is arbitrarily taken to be $\theta = 5\times 10^{-8}$ rad. Two principal vectors $\mathbf{w}_8$ and $\mathbf{w}_{10}$ are coupled to $\mathbf{v}_7$ and $\mathbf{v}_9$, respectively and are found using the MATLAB *rref* command on the augmented matrix, again as described by Stephen and Wang (1996), followed by appropriate interpretation. Principal vector $\mathbf{w}_8$, consists of the necessary combination of tensile force and twisting moment which, when applied to the left- and right-hand sides of the cell, produces the unit extension defined by eigenvector $\mathbf{v}_7$ on the right. Principal vector $\mathbf{w}_{10}$ consists of the necessary combination of twisting moment and tensile force which, when applied to the left- and right-hand sides of the cell, produces the rotation defined by eigenvector $\mathbf{v}_9$ on the right. Two 2×2 Jordan blocks are associated with these vectors, which are

$$\mathbf{J}^{(1)}_{2\times 2} = \mathbf{J}^{(2)}_{2\times 2} = \begin{bmatrix}1 & 1\\ 0 & 1\end{bmatrix}. \tag{24}$$

A variety of strategies are possible for determination of the eigen- and principal vectors associated with the multiple complex unity eigenvalues, $4\times \mathrm{e}^{\pm \mathrm{i}\alpha}$. For example, two chains of equations relating eigen- and principal vectors may be expressed as

$$\begin{aligned}
&(\mathbf{G}'-\mathrm{e}^{\mathrm{i}\alpha}\mathbf{I})\mathbf{v}_{11} = 0 \quad (\mathbf{G}'-\mathrm{e}^{-\mathrm{i}\alpha}\mathbf{I})\mathbf{v}_{15} = 0,\\
&(\mathbf{G}'-\mathrm{e}^{\mathrm{i}\alpha}\mathbf{I})\mathbf{w}_{12} = \mathbf{v}_{11} \quad (\mathbf{G}'-\mathrm{e}^{-\mathrm{i}\alpha}\mathbf{I})\mathbf{w}_{16} = \mathbf{v}_{15},\\
&(\mathbf{G}'-\mathrm{e}^{\mathrm{i}\alpha}\mathbf{I})\mathbf{w}_{13} = \mathbf{w}_{12} \quad (\mathbf{G}'-\mathrm{e}^{-\mathrm{i}\alpha}\mathbf{I})\mathbf{w}_{17} = \mathbf{w}_{16},\\
&(\mathbf{G}'-\mathrm{e}^{\mathrm{i}\alpha}\mathbf{I})\mathbf{w}_{14} = \mathbf{w}_{13} \quad (\mathbf{G}'-\mathrm{e}^{-\mathrm{i}\alpha}\mathbf{I})\mathbf{w}_{18} = \mathbf{w}_{17}.
\end{aligned} \tag{25}$$

The reduced row echelon forms of the matrices $(\mathbf{G}'-\mathrm{e}^{\mathrm{i}\alpha}\mathbf{I})$ and $(\mathbf{G}'-\mathrm{e}^{-\mathrm{i}\alpha}\mathbf{I})$, respectively, yields the two eigenvectors

$$\mathbf{v}_{11} = [0\ \ \mathrm{i}\ \ 1\ \ 0\ \ \mathrm{i}\ \ 1\ \ 0\ \ \mathrm{i}\ \ 1\ \ 0\ \ 0\ \ 0\ \ 0\ \ 0\ \ 0\ \ 0\ \ 0\ \ 0]^{\mathrm{T}}\times 10^{-8}, \tag{26}$$

$$\mathbf{v}_{15} = [0\ \ -\mathrm{i}\ \ 1\ \ 0\ \ -\mathrm{i}\ \ 1\ \ 0\ \ -\mathrm{i}\ \ 1\ \ 0\ \ 0\ \ 0\ \ 0\ \ 0\ \ 0\ \ 0\ \ 0\ \ 0]^{\mathrm{T}}\times 10^{-8}, \tag{27}$$

which are a combination of real and imaginary rigid body displacements in the y- and z-directions. The principal vectors $\mathbf{w}_{12}$ to $\mathbf{w}_{14}$ and $\mathbf{w}_{16}$ to $\mathbf{w}_{18}$ can then be determined by following the chains, Eqs. (25). If one then constructs a similarity matrix $\mathbf{V}$ from these eigen- and principal vectors, this gives the Jordan canonical form (JCF) at its simplest

$$\mathbf{J}=\mathbf{V}^{-1}\mathbf{G}'\mathbf{V}=\begin{bmatrix}\lambda_1 & 0 & 0 & 0 & 0 & 0 & 0 & 0 & 0 & 0\\ 0 & \lambda_2 & 0 & 0 & 0 & 0 & 0 & 0 & 0 & 0\\ 0 & 0 & \bar{\lambda}_2 & 0 & 0 & 0 & 0 & 0 & 0 & 0\\ 0 & 0 & 0 & \lambda_1^{-1} & 0 & 0 & 0 & 0 & 0 & 0\\ 0 & 0 & 0 & 0 & \lambda_2^{-1} & 0 & 0 & 0 & 0 & 0\\ 0 & 0 & 0 & 0 & 0 & \bar{\lambda}_2^{-1} & 0 & 0 & 0 & 0\\ 0 & 0 & 0 & 0 & 0 & 0 & \mathbf{J}^{(1)}_{2\times 2} & 0 & 0 & 0\\ 0 & 0 & 0 & 0 & 0 & 0 & 0 & \mathbf{J}^{(2)}_{2\times 2} & 0 & 0\\ 0 & 0 & 0 & 0 & 0 & 0 & 0 & 0 & \mathbf{J}^{(1)}_{4\times 4} & 0\\ 0 & 0 & 0 & 0 & 0 & 0 & 0 & 0 & 0 & \mathbf{J}^{(2)}_{4\times 4}\end{bmatrix}, \tag{28}$$

where the two 4×4 Jordan blocks associated with the multiple complex unity eigenvalues are

$$\mathbf{J}^{(1)}_{4\times 4}=\begin{bmatrix}e^{i\alpha} & 1 & 0 & 0\\ 0 & e^{i\alpha} & 1 & 0\\ 0 & 0 & e^{i\alpha} & 1\\ 0 & 0 & 0 & e^{i\alpha}\end{bmatrix},\quad \mathbf{J}^{(2)}_{4\times 4}=\begin{bmatrix}e^{-i\alpha} & 1 & 0 & 0\\ 0 & e^{-i\alpha} & 1 & 0\\ 0 & 0 & e^{-i\alpha} & 1\\ 0 & 0 & 0 & e^{-i\alpha}\end{bmatrix}. \tag{29a, b}$$

Now, while the JCF may be in its simplest form, because of the complex eigenvalues, and complex eigen- and principal vectors, interpretation of the vectors is at its most difficult. A complex vector is not physically permissible, but when considered in conjunction with its conjugate, the (real) displacement and force components are the real and imaginary parts, in turn. Indeed, if one replaces the complex conjugate columns of the similarity matrix by their real and imaginary parts, one obtains the real JCF

$$\mathbf{J}=\begin{bmatrix}\lambda_1 & 0 & 0 & 0 & 0 & 0 & 0 & 0 & 0\\ 0 & \mathrm{real}(\lambda_2) & -\mathrm{imag}(\lambda_2) & 0 & 0 & 0 & 0 & 0 & 0\\ 0 & \mathrm{imag}(\lambda_2) & \mathrm{real}(\lambda_2) & 0 & 0 & 0 & 0 & 0 & 0\\ 0 & 0 & 0 & \lambda_1^{-1} & 0 & 0 & 0 & 0 & 0\\ 0 & 0 & 0 & 0 & \mathrm{real}(\bar{\lambda}_2) & -\mathrm{imag}(\bar{\lambda}_2) & 0 & 0 & 0\\ 0 & 0 & 0 & 0 & \mathrm{imag}(\bar{\lambda}_2) & \mathrm{real}(\bar{\lambda}_2) & 0 & 0 & 0\\ 0 & 0 & 0 & 0 & 0 & 0 & \mathbf{J}^{(1)}_{2\times 2} & 0 & 0\\ 0 & 0 & 0 & 0 & 0 & 0 & 0 & \mathbf{J}^{(2)}_{2\times 2} & 0\\ 0 & 0 & 0 & 0 & 0 & 0 & 0 & 0 & \mathbf{J}_{8\times 8}\end{bmatrix}, \tag{30}$$

where

$$\mathbf{J}_{8\times 8} = \begin{bmatrix} c & -s & 1 & 0 & 0 & 0 & 0 & 0 \\ s & c & 0 & 1 & 0 & 0 & 0 & 0 \\ 0 & 0 & c & -s & 1 & 0 & 0 & 0 \\ 0 & 0 & s & c & 0 & 1 & 0 & 0 \\ 0 & 0 & 0 & 0 & c & -s & 1 & 0 \\ 0 & 0 & 0 & 0 & s & c & 0 & 1 \\ 0 & 0 & 0 & 0 & 0 & 0 & c & -s \\ 0 & 0 & 0 & 0 & 0 & 0 & s & c \end{bmatrix}, \tag{31}$$

with $c = \cos\alpha$, $s = \sin\alpha$; note that the single complex unity eigenvalues on the leading diagonal are replaced by 2×2 real blocks. Within this formulation, the principal vectors $\mathbf{w}_{13}$ and $\mathbf{w}_{14}$ describe rigid body rotations of the left-hand side of the cell, but employ the local y'- and z'-axes of the right-hand cross-section, respectively. In turn, their coupled principal vectors $\mathbf{w}_{15}$, $\mathbf{w}_{16}$, $\mathbf{w}_{17}$ and $\mathbf{w}_{18}$ describe bending moment and shear vectors applied to the left-hand side of the cell, but employ the local coordinate system of the right-hand side of the cell. For interpretation of these vectors, it is easier if they are expressed within the local coordinate system of the left-hand side, for which the local and global coordinate systems coincide. This is achieved by employing a near diagonal Jordan decomposition in which the complex unity eigenvalue replaces the real unity on the super diagonal; the chains then become

$$\begin{aligned} &(\mathbf{G}' - \mathrm{e}^{\mathrm{i}\alpha}\mathbf{I})\mathbf{v}_{11} = 0, && (\mathbf{G}' - \mathrm{e}^{-\mathrm{i}\alpha}\mathbf{I})\mathbf{v}_{15} = 0, \\ &(\mathbf{G}' - \mathrm{e}^{\mathrm{i}\alpha}\mathbf{I})\mathbf{w}_{12} = \mathrm{e}^{\mathrm{i}\alpha}\mathbf{v}_{11}, && (\mathbf{G}' - \mathrm{e}^{-\mathrm{i}\alpha}\mathbf{I})\mathbf{w}_{16} = \mathrm{e}^{-\mathrm{i}\alpha}\mathbf{v}_{15}, \\ &(\mathbf{G}' - \mathrm{e}^{\mathrm{i}\alpha}\mathbf{I})\mathbf{w}_{13} = \mathrm{e}^{\mathrm{i}\alpha}\mathbf{w}_{12}, && (\mathbf{G}' - \mathrm{e}^{-\mathrm{i}\alpha}\mathbf{I})\mathbf{w}_{17} = \mathrm{e}^{-\mathrm{i}\alpha}\mathbf{w}_{16}, \\ &(\mathbf{G}' - \mathrm{e}^{\mathrm{i}\alpha}\mathbf{I})\mathbf{w}_{14} = \mathrm{e}^{\mathrm{i}\alpha}\mathbf{w}_{13}, && (\mathbf{G}' - \mathrm{e}^{-\mathrm{i}\alpha}\mathbf{I})\mathbf{w}_{18} = \mathrm{e}^{-\mathrm{i}\alpha}\mathbf{w}_{17}. \end{aligned} \tag{32}$$

The new complex similarity matrix $\mathbf{V}$ comprised of these eigen- and principal vectors transforms the transfer matrix $\mathbf{G}'$ into a new JCF, which remains broadly as in Eq. (28), but with two new $4 \cdot 4$ blocks, which are

$$\mathbf{J}^{(1)}_{4\times 4} = \begin{bmatrix} \mathrm{e}^{\mathrm{i}\alpha} & \mathrm{e}^{\mathrm{i}\alpha} & 0 & 0 \\ 0 & \mathrm{e}^{\mathrm{i}\alpha} & \mathrm{e}^{\mathrm{i}\alpha} & 0 \\ 0 & 0 & \mathrm{e}^{\mathrm{i}\alpha} & \mathrm{e}^{\mathrm{i}\alpha} \\ 0 & 0 & 0 & \mathrm{e}^{\mathrm{i}\alpha} \end{bmatrix}, \quad \mathbf{J}^{(2)}_{4\times 4} = \begin{bmatrix} \mathrm{e}^{-\mathrm{i}\alpha} & \mathrm{e}^{-\mathrm{i}\alpha} & 0 & 0 \\ 0 & \mathrm{e}^{-\mathrm{i}\alpha} & \mathrm{e}^{-\mathrm{i}\alpha} & 0 \\ 0 & 0 & \mathrm{e}^{-\mathrm{i}\alpha} & \mathrm{e}^{-\mathrm{i}\alpha} \\ 0 & 0 & 0 & \mathrm{e}^{-\mathrm{i}\alpha} \end{bmatrix}. \tag{33}$$

Again, this leads to complex conjugate eigen- and principal vectors, and replacing these by their real and imaginary parts, allows one to construct a new real similarity matrix which transforms $\mathbf{G}'$ into a new real JCF, which differs from Eq. (31), in that the 8×8 block becomes

$$\mathbf{J}_{8\times 8} = \begin{bmatrix} c & -s & c & -s & 0 & 0 & 0 & 0 \\ s & c & s & c & 0 & 0 & 0 & 0 \\ 0 & 0 & c & -s & c & -s & 0 & 0 \\ 0 & 0 & s & c & s & c & 0 & 0 \\ 0 & 0 & 0 & 0 & c & -s & c & -s \\ 0 & 0 & 0 & 0 & s & c & s & c \\ 0 & 0 & 0 & 0 & 0 & 0 & c & -s \\ 0 & 0 & 0 & 0 & 0 & 0 & s & c \end{bmatrix}. \tag{34}$$

This real similarity matrix **V** and the associated JCF are given in Appendix A. The eigen- and principal vectors pertaining to the multiple complex unity eigenvalues are now expressed within the global coordinate system of the left-hand cross-section. This greatly simplifies the physical interpretation of these vectors and, in turn, determination of the equivalent continuum properties.

5. Equivalent continuum properties

5.1. Tension–torsion coupling

The two vectors $\mathbf{v}_7$ and $\mathbf{w}_8$ are coupled according to

$$\mathbf{G}'\mathbf{w}_8 = \mathbf{w}_8 + \mathbf{v}_7 \tag{35}$$

as shown in Fig. 4, where it is seen that a tensile force and a twisting moment are applied on both hand sides of the cell in order to produce unit extension in the x-direction, only. The two vectors $\mathbf{v}_9$ and $\mathbf{w}_{10}$ are coupled according to

$$\mathbf{G}'\mathbf{w}_{10} = \mathbf{w}_{10} + \mathbf{v}_9 \tag{36}$$

as shown in Fig. 5, where it is seen that a twisting moment and a compressive force are applied on both sides of the cell in order to produce rotation about the x-axis, only. Following Di Prima (1959), tension–torsion coupling is expressed as

$$\begin{bmatrix} T \\ M_x \end{bmatrix} = \begin{bmatrix} EA & K_{tt} \\ K_{tt} & GJ \end{bmatrix} \begin{bmatrix} u/L \\ \theta/L \end{bmatrix} \tag{37}$$

where K_{tt} is the coupling coefficient. From vectors $\mathbf{w}_8$ and $\mathbf{v}_7$, the quantities T, M_x and u are known (θ is zero), and the equivalent cross-sectional area and coupling coefficient are calculated as $A = (0.22941 \times 0.3428)/(70 \times 10^9 \times 1 \times 10^{-8}) = 1.1234 \times 10^{-4}\ \mathrm{m}^2$, and $K_{tt} = -1.8578 \times 10^5\ \mathrm{N\,m}$. Additionally, there is a Poisson's ratio effect on the cross-section; the strain in the x-direction is $\varepsilon_x = 1 \times 10^{-8}\ /0.3428 = 2.9172 \times 10^{-8}$, while the strains in the y- and z-directions are $\varepsilon_y = (-1.6883 - 0.8442) \times 10^{-9}/(0.3428 \times \sqrt{3}/2) = -8.5306 \times 10^{-9}, \varepsilon_z = -(1.6214 \times 10^{-9})/0.3428 = -8.5306 \times 10^{-9}$. Employing $v = -\varepsilon_y/\varepsilon_x =$

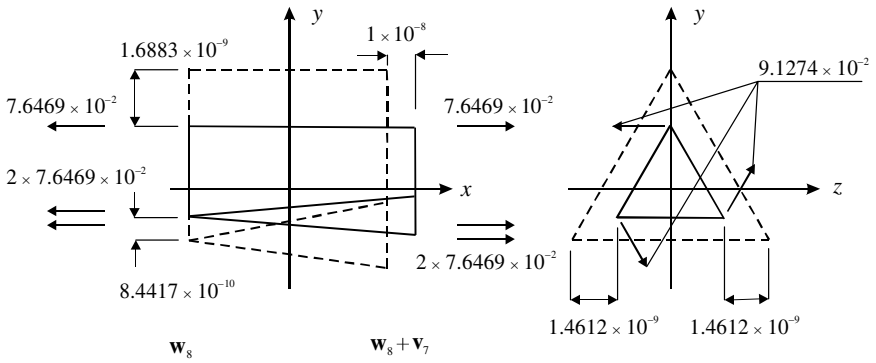

Fig. 4. Coupling of eigenvector $\mathbf{v}_7$, for rigid body displacement in the x-direction, with principal vector $\mathbf{w}_8$ for extension: displacements are exaggerated. Dotted lines show initial configuration.

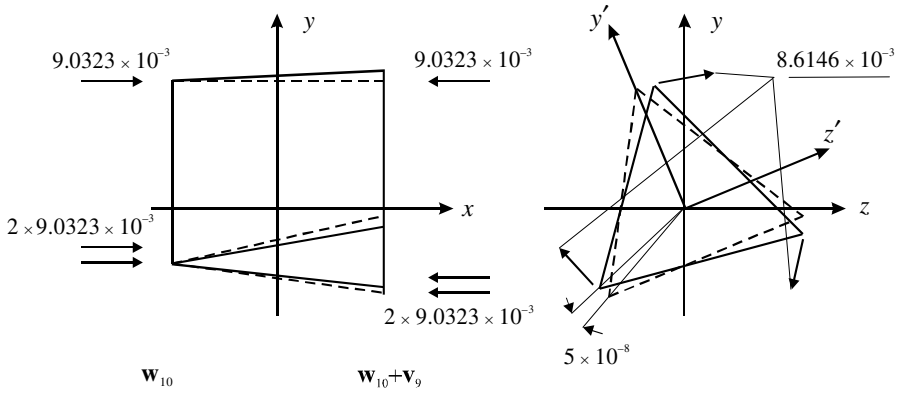

Fig. 5. Coupling of eigenvector $\mathbf{v}_9$ for rigid body rotation about the x-axis, with principal vector $\mathbf{w}_{10}$ for torsion.

$-\varepsilon_z/\varepsilon_x$, the Poisson's ratio is calculated as $\nu = 0.2924$. In turn, an equivalent shear modulus is found as $G = E/(2(1+\nu)) = 27.081 \times 10^9$ N/m^2, with Young's modulus E being regarded as invariant.

From vectors $\mathbf{w}_{10}$ and $\mathbf{v}_9$, quantities T, M_x and θ are known (u is zero), and Eq. (37) give the equivalent torsion constant and coupling coefficient as $J = (8.6146 \times 10^{-3} \times 0.3428/\sqrt{3})/\ (27.081 \times 10^9 \times 5 \times 10^{-8}) = 1.2949 \times 10^{-6}$ m^4, and $K_{tt} = -1.8578\ \times 10^5$ Nm, respectively; the latter is identical to that found from vectors $\mathbf{w}_8$ and $\mathbf{v}_7$, as one would expect from the reciprocal theorem.

5.2. Rigid body rotations

The two principal vectors $\mathbf{w}_{13}$ and $\mathbf{w}_{14}$ are coupled to the rigid body displacement eigenvectors $\mathbf{v}_{11}$ and $\mathbf{v}_{12}$ according to the scheme

$$\begin{aligned}\mathbf{G}'\mathbf{w}_{13} &= \mathbf{v}_{11}\cos\alpha + \mathbf{v}_{12}\sin\alpha + \mathbf{w}_{13}\cos\alpha + \mathbf{w}_{14}\sin\alpha,\\ \mathbf{G}'\mathbf{w}_{14} &= -\mathbf{v}_{11}\sin\alpha + \mathbf{v}_{12}\cos\alpha - \mathbf{w}_{13}\sin\alpha + \mathbf{w}_{14}\cos\alpha.\end{aligned} \tag{38a, b}$$

Vectors $\mathbf{w}_{13}$ and $\mathbf{w}_{14}$ describe rigid body rotations of the left-hand cross-section about the z- and y-axes, respectively, within the global coordinate system. Pre-multiplication of these vectors by the transfer matrix $\mathbf{G}'$ will give rigid body rotations of the right-hand side about the local z'- and y'-axes, respectively, as indicated by Eq. (14). However interpretation of these vectors is easier when these right-hand rotations are expressed within the global coordinate system, which is achieved by pre-multiplication by $\mathbf{G}$, according to

$$\mathbf{w}_{13\mathbf{R}} = \mathbf{G}\mathbf{w}_{13}, \mathbf{w}_{14\mathbf{R}} = \mathbf{G}\mathbf{w}_{14} \tag{39}$$

where $\mathbf{G}$ is the transfer matrix defined within the global coordinate system for this first cell, and the additional subscript $\mathbf{R}$ denotes the right-hand side vector; these vectors are shown in Fig. 6.

5.3. Bending moments

Principal vectors $\mathbf{w}_{15}$ and $\mathbf{w}_{16}$ describe the bending moments on the left-hand side of the cell in the xy- and xz-planes, respectively, within the global coordinate system, and are coupled to the rotations according to

$$\begin{aligned}\mathbf{G}'\mathbf{w}_{15} &= \mathbf{w}_{13}\cos\alpha + \mathbf{w}_{14}\sin\alpha + \mathbf{w}_{15}\cos\alpha + \mathbf{w}_{16}\sin\alpha,\\ \mathbf{G}'\mathbf{w}_{16} &= -\mathbf{w}_{13}\sin\alpha + \mathbf{w}_{14}\cos\alpha - \mathbf{w}_{15}\sin\alpha + \mathbf{w}_{16}\cos\alpha.\end{aligned} \tag{40a, b}$$

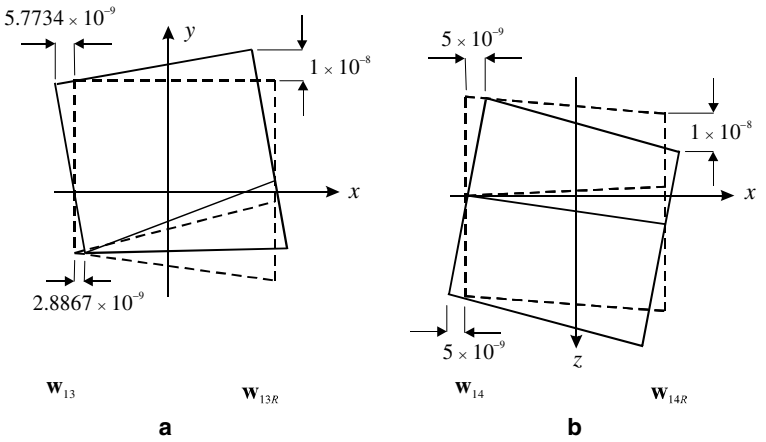

Fig. 6. (a) Principal vector $\mathbf{w}_{13}$ for rigid body rotation about the z-axis: (b) principal vector $\mathbf{w}_{14}$ for rigid body rotation about the y-axis.

Again, pre-multiplication by $\mathbf{G}'$ would give the two bending moment vectors on the right-hand side of the cell in the local $x'y'$- and $x'z'$-planes, and for interpretation of the vectors, it is preferable that these right-hand vectors be expressed within the global coordinate system, which is achieved by pre-multiplication by $\mathbf{G}$, to give

$$\mathbf{w}_{15\mathrm{R}} = \mathbf{G}\mathbf{w}_{15}, \quad \mathbf{w}_{16\mathrm{R}} = \mathbf{G}\mathbf{w}_{16}. \tag{41}$$

Analysis of the x-direction displacement components of the left-hand cross-section within vectors $\mathbf{w}_{15}$ and $\mathbf{w}_{16}$, shows that both are comprised of two rotations about the y- and z-axes, and can be decomposed as

$$\begin{bmatrix} d_{1x} \\ d_{2x} \\ d_{3x} \end{bmatrix}^{\mathbf{w}_{15}} = a \times \begin{bmatrix} d_{1x} \\ d_{2x} \\ d_{3x} \end{bmatrix}^{\mathbf{w}_{13}} + b \times \begin{bmatrix} d_{1x} \\ d_{2x} \\ d_{3x} \end{bmatrix}^{\mathbf{w}_{4}}, \quad \begin{bmatrix} d_{1x} \\ d_{2x} \\ d_{3x} \end{bmatrix}^{\mathbf{w}_{16}} = c \times \begin{bmatrix} d_{1x} \\ d_{2x} \\ d_{3x} \end{bmatrix}^{\mathbf{w}_{14}} + d \times \begin{bmatrix} d_{1x} \\ d_{2x} \\ d_{3x} \end{bmatrix}^{\mathbf{w}_{13}}. \tag{42a, b}$$

Similar analysis of these components within the right-hand side vectors $\mathbf{w}_{15\mathrm{R}}$ and $\mathbf{w}_{16\mathrm{R}}$, shows that they are also comprised of two rotations about the y- and z-axes, and can be decomposed as

$$\begin{bmatrix} d_{4x} \\ d_{5x} \\ d_{6x} \end{bmatrix}^{\mathbf{w}_{15\mathrm{R}}} = e \times \begin{bmatrix} d_{4x} \\ d_{5x} \\ d_{6x} \end{bmatrix}^{\mathbf{w}_{13\mathrm{R}}} + f \times \begin{bmatrix} d_{4x} \\ d_{5x} \\ d_{6x} \end{bmatrix}^{\mathbf{w}_{14\mathrm{R}}}, \quad \begin{bmatrix} d_{4x} \\ d_{5x} \\ d_{6x} \end{bmatrix}^{\mathbf{w}_{16\mathrm{R}}} = g \times \begin{bmatrix} d_{4x} \\ d_{5x} \\ d_{6x} \end{bmatrix}^{\mathbf{w}_{14\mathrm{R}}} + h \times \begin{bmatrix} d_{4x} \\ d_{5x} \\ d_{6x} \end{bmatrix}^{\mathbf{w}_{13\mathrm{R}}}. \tag{43a, b}$$

Simple calculations from Eqs. (42) and (43) give $a = -0.5$, $b = 0.2109$, $c = -0.5$ and $d = -0.2109$, for the left-hand side, and $e = 0.5$, $f = 0.2109$, $g = 0.5$ and $h = -0.2109$ for the right; the fact that coefficients a and e are equal but of opposite sign indicates a curvature of the cell, while the equality of coefficients b and f indicates a shear deformation of the cell, as shown in Figs. 7 and 8. From Figs. 7(a) and 8(a), the two bending curvatures in the xy- and xz-planes, respectively, are

$$\begin{aligned} \frac{1}{R_y} &= \frac{\partial \psi_z}{\partial x} = 1.4434 \times 10^{-9} \Big/ \left(\frac{H}{3} \times \frac{L}{2}\right) = 8.5098 \times 10^{-8}\ \mathrm{m}^{-1}, \\ \frac{1}{R_z} &= \frac{\partial \psi_y}{\partial x} = 2.5 \times 10^{-9} \Big/ \left(\frac{L}{2} \times \frac{L}{2}\right) = 8.5098 \times 10^{-8}\ \mathrm{m}^{-1}, \end{aligned} \tag{44a, b}$$

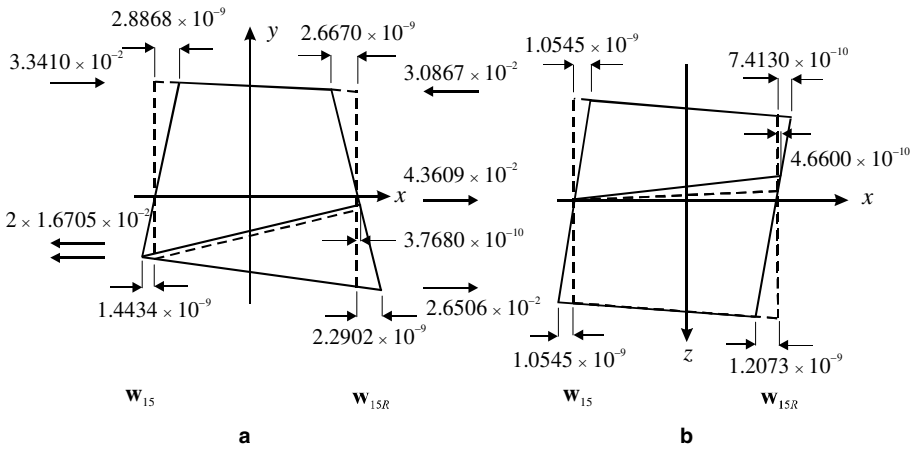

Fig. 7. Principal vector $\mathbf{w}_{15}$ for bending moment in the xy-plane: (a) and (b) show the displacement and force components in the xy- and xz-planes, respectively.

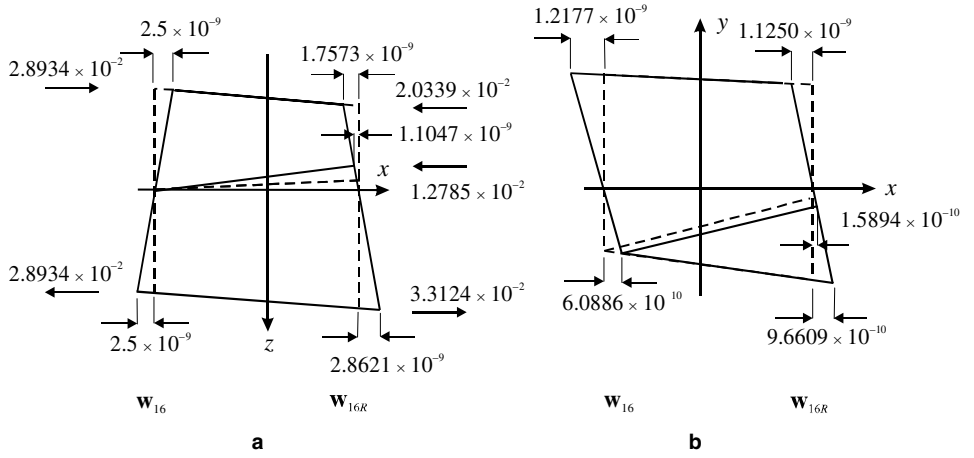

Fig. 8. Principal vector $\mathbf{w}_{16}$, for bending moment in the xz-plane: (a) and (b) show the displacement and force components in the xz- and xy-planes, respectively.

while consideration of Figs. 7(b) and 8(b) gives the two coupled shear angles in the xz- and xy-planes, respectively, as

$$\gamma_{xz} = 1.0546 \times 10^{-9}/(L/2) = 6.1527 \times 10^{-9},$$
$$\gamma_{xy} = 6.0886 \times 10^{-10}/6.0886 \times 10^{-10}/(H/2) = 6.1527 \times 10^{-9}. \quad (45a, b)$$

The above indicates that a bending moment produces a curvature in the plane of bending, together with a shear deformation in the perpendicular plane, and is consistent with the bending theory of pre-twisted beams presented by Tabarrok and Xiong (1989). It should be noted that the bending moment vectors also contain self-equilibrating nodal forces in the y- and z-directions, although these are not shown in Figs. 7 and 8, which implies that the resultant nodal force is not in the axial direction. Such additional components of force are not required from consideration of force or moment equilibrium, but rather from nodal

displacement compatibility requirements of adjacent cells. In contrast to many theories of pre-twisted beams, there is no evidence of bending–bending coupling, that is, curvature in two perpendicular planes produced by the moment.

5.4. Shearing forces

Principal vectors $\mathbf{w}_{17}$ and $\mathbf{w}_{18}$ are coupled to the bending moments on the left-hand side of the cell, according to

$$\begin{aligned}\mathbf{G}'\mathbf{w}_{17} &= \mathbf{w}_{15}\cos\alpha + \mathbf{w}_{16}\sin\alpha + \mathbf{w}_{17}\cos\alpha + \mathbf{w}_{18}\sin\alpha,\\ \mathbf{G}'\mathbf{w}_{18} &= -\mathbf{w}_{15}\sin\alpha + \mathbf{w}_{16}\cos\alpha - \mathbf{w}_{17}\sin\alpha + \mathbf{w}_{18}\cos\alpha.\end{aligned} \tag{46a, b}$$

Previous experience from the eigenanalysis of a straight repetitive structure suggests that these two vectors should describe shear; however analysis of the force components within vectors w_{17} and w_{18} gives a resultant shear force Q_y, and moments M_z, M_y for the former, and a resultant shear force Q_z, and moments M_y, M_z for the latter. In fact, only Q_y and M_z, and Q_z and M_y are required to define the simplest left-hand shear vectors in the xy- and xz-planes, respectively, such that one should have a shearing force only on the right-hand side of the cell, and the unnecessary bending moments are removed according to the scheme

$$\begin{aligned}\mathbf{w}^*_{17} &= \mathbf{w}_{17} - \frac{\text{resultant}(M_y)\ \text{within}\ \mathbf{w}_{17}}{\text{resultant}(M_y)\ \text{within}\ \mathbf{w}_{16}} \times \mathbf{w}_{16},\\ \mathbf{w}^*_{18} &= \mathbf{w}_{17} - \frac{\text{resultant}(M_z)\ \text{within}\ \mathbf{w}_{18}}{\text{resultant}(M_z)\ \text{within}\ \mathbf{w}_{15}} \times \mathbf{w}_{15}.\end{aligned} \tag{47a, b}$$

The two new shear vectors $\mathbf{w}^*_{17}$ and $\mathbf{w}^*_{18}$ are given in Appendix B. Again, it is preferable that the shear vectors on the right-hand side of the cell should be given within the global coordinate system, and these are determined by

$$\mathbf{w}^*_{17\mathrm{R}} = \mathbf{G}\mathbf{w}^*_{17}, \quad \mathbf{w}^*_{18\mathrm{R}} = \mathbf{G}\mathbf{w}^*_{18}; \tag{48}$$

these describe the shear vectors in the xy- and xz-planes on both sides of the single cell, in global coordinates, in their simplest forms.

Again, consideration of the x-direction displacement components in the left-hand side vectors $\mathbf{w}^*_{17}$ and $\mathbf{w}^*_{18}$ shows that they can be decomposed into rotations about the y- and z-axes, as

$$\begin{bmatrix} d_{1x}\\ d_{2x}\\ d_{3x}\end{bmatrix}^{\mathbf{w}^*_{17}} = a \times \begin{bmatrix} d_{1x}\\ d_{2x}\\ d_{3x}\end{bmatrix}^{\mathbf{w}_{13}} + b \times \begin{bmatrix} d_{1x}\\ d_{2x}\\ d_{3x}\end{bmatrix}^{\mathbf{w}_{14}}, \quad \begin{bmatrix} d_{1x}\\ d_{2x}\\ d_{3x}\end{bmatrix}^{\mathbf{w}^*_{18}} = c \times \begin{bmatrix} d_{1x}\\ d_{2x}\\ d_{3x}\end{bmatrix}^{\mathbf{w}_{14}} + d \times \begin{bmatrix} d_{1x}\\ d_{2x}\\ d_{3x}\end{bmatrix}^{\mathbf{w}_{13}}, \tag{49a, b}$$

while, consideration of these components in the right-hand side vectors $\mathbf{w}^*_{17\mathrm{R}}$ and $\mathbf{w}^*_{18\mathrm{R}}$ shows that they are also comprised of rotations about the y- and z-axes, as

$$\begin{bmatrix} d_{4x}\\ d_{5x}\\ d_{6x}\end{bmatrix}^{\mathbf{w}^*_{17\mathrm{R}}} = e \times \begin{bmatrix} d_{4x}\\ d_{5x}\\ d_{6x}\end{bmatrix}^{\mathbf{w}_{13\mathrm{R}}} + f \times \begin{bmatrix} d_{4x}\\ d_{5x}\\ d_{6x}\end{bmatrix}^{\mathbf{w}_{14\mathrm{R}}}, \quad \begin{bmatrix} d_{4x}\\ d_{5x}\\ d_{6x}\end{bmatrix}^{\mathbf{w}^*_{18\mathrm{R}}} = g \times \begin{bmatrix} d_{4x}\\ d_{5x}\\ d_{6x}\end{bmatrix}^{\mathbf{w}_{14\mathrm{R}}} + h \times \begin{bmatrix} d_{4x}\\ d_{5x}\\ d_{6x}\end{bmatrix}^{\mathbf{w}_{13\mathrm{R}}}. \tag{50a, b}$$

Again, simple calculations from Eqs. (49) and (50) gives $a = 1.1678$, $b = 0.0307$, $c = 1.1678$ and $d = -0.0307$ on the left-hand side, and $e = 0.6678$, $f = -0.2416$, $g = 0.6678$ and $h = 0.2416$ on the right. These shear vectors $\mathbf{w}^*_{17}$ and $\mathbf{w}^*_{17\mathrm{R}}$, and $\mathbf{w}^*_{18}$ and $\mathbf{w}^*_{18\mathrm{R}}$ are shown in Figs. 9 and 10, respectively; the x-direction

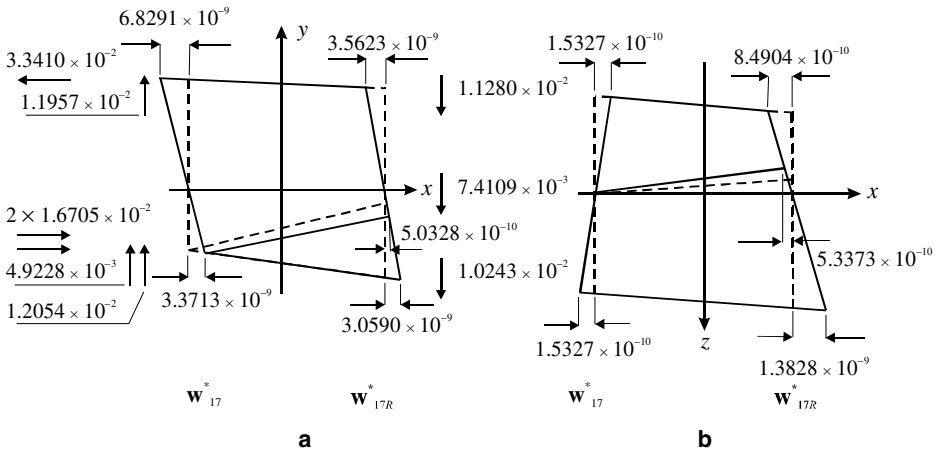

Fig. 9. Principal vector $\mathbf{w}^*_{17}$ for shearing force and bending moment in the, xy-plane: (a) and (b) show the displacement and force components in the xy- and xz-planes. respectively.

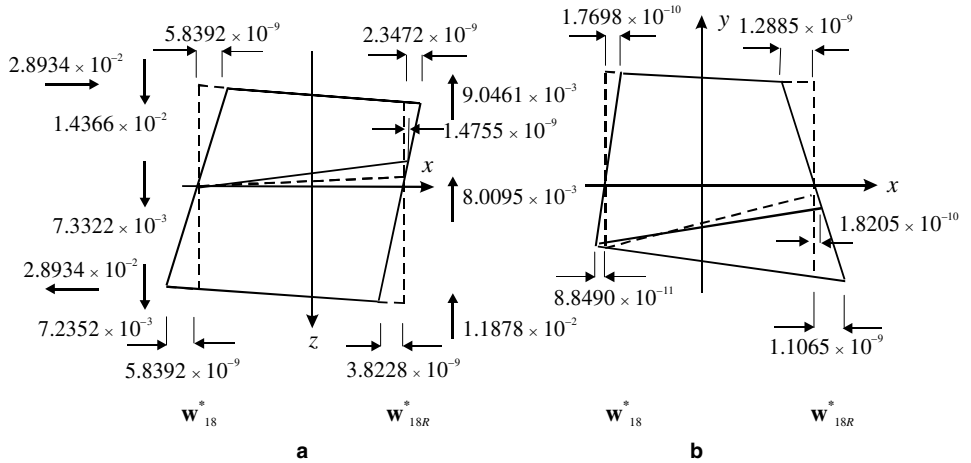

Fig. 10. Principal vector $\mathbf{w}^*_{18}$ for shearing force and bending moment in the xz-plane: (a) and (b) show the displacement and force components in the xz- and xy-planes, respectively.

displacement components within the vectors can be further decomposed, as illustrated in Figs. 11–14, which indicate the intricacy of the coupling.

The combination of shearing force and bending moment described by vector $\mathbf{w}^*_{17}$, Fig. 9, may be regarded as producing the primary deformations of a shear angle and a curvature in the xy-plane, Fig. 11; this is the expected behaviour of a straight beam. Coupled to these are secondary deformations of a curvature, Fig. 12(a), and a shear angle, Fig. 12(b), in the xz-plane. One would expect the former by virtue of the reciprocal theorem: in vector $\mathbf{w}_{16}$ one has the primary response of a curvature in the xz-plane, and the coupled secondary response of a shear angle in the xy-plane. On the other hand, the secondary shear angle in the xz-plane may be regarded as a repeat of the curvature-shear coupling exhibited in the bending moment vector $\mathbf{w}_{15}$, as the shear vector contains a bending moment. Indeed, as will be seen, these

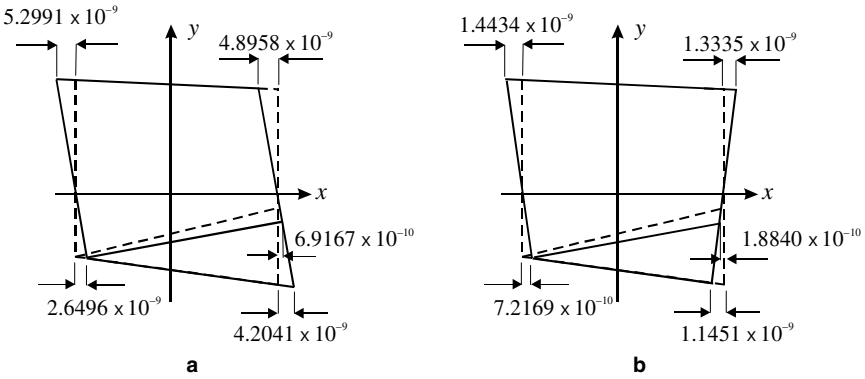

Fig. 11. Decomposition of the displacements in the *xy*-plane of Fig. 9: (a) shows the shear angle due to shearing force and (b) shows the bending curvature due to bending moment.

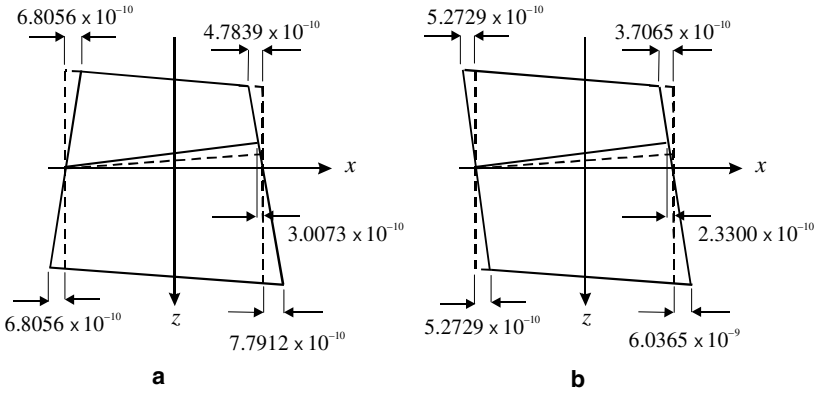

Fig. 12. Decomposition of the displacements in the *xz*-plane of Fig. 9: (a) shows the bending curvature coupled with the shear angle in the, *xz*-plane due to shearing force and (b) shows the shear angle coupled with the bending curvature in the, *xz*-plane due to bending moment.

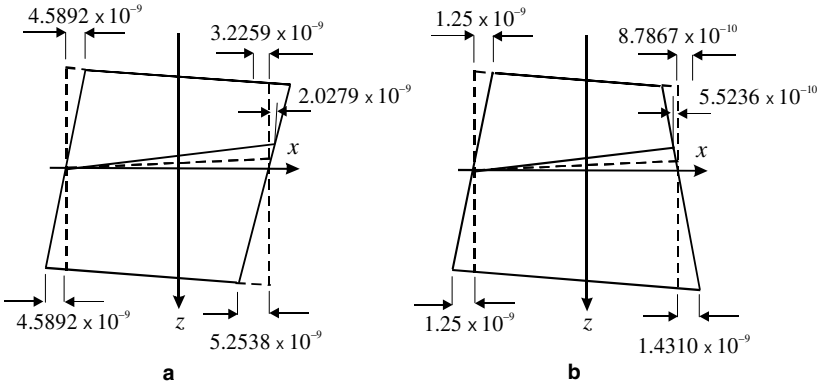

Fig. 13. Decomposition of the displacements in the *xz*-plane of Fig. 10: (a) shows the shear angle due to shearing force and (b) shows the bending curvature due to bending moment.

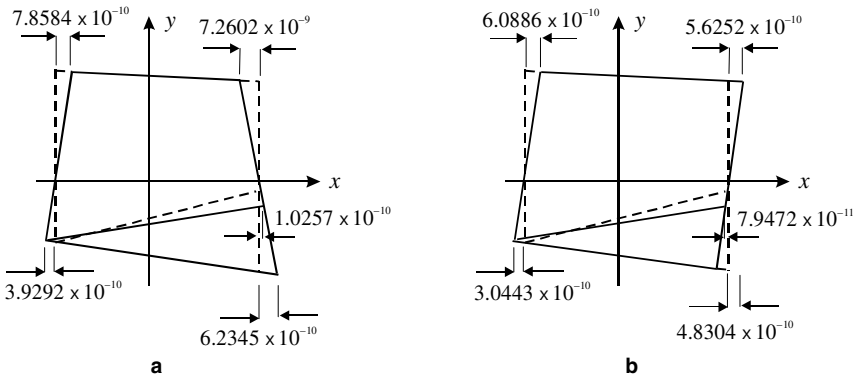

Fig. 14. Decomposition of the displacements in the xy-plane of Fig. 10: (a) shows the bending curvature coupled with the shear angle in the xy-plane due to shearing force and (b) shows the shear angle coupled with the bending curvature in the xy-plane due to bending moment.

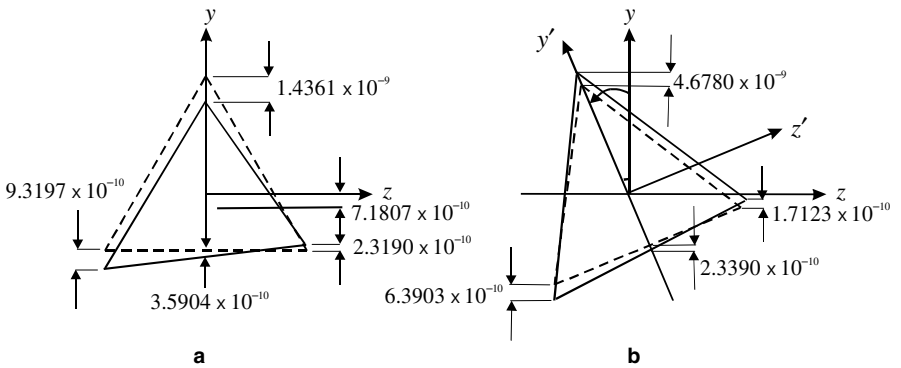

Fig. 15. Displacements in the y-direction for the principal vector $\mathbf{w}_{17}^{*}$ on the left-hand (a) and right-hand (b) sides of the cell, respectively.

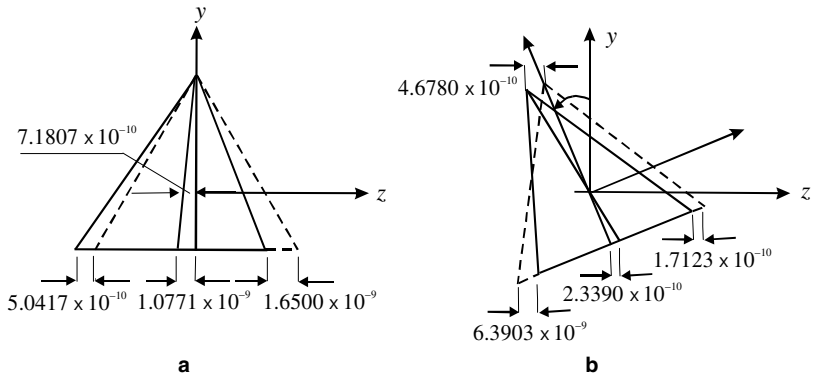

Fig. 16. Displacements in the z-direction for the principal vector $\mathbf{w}_{18}^{*}$ ls on the left-hand (a) and right-hand (b) sides of the cell, respectively.

are exactly one half of those associated with $\mathbf{w}_{15}$, as one might expect: for a continuum, a shearing force induces a bending moment which varies linearly along the length, whose effect should be one-half that of a pure moment, the latter being constant along the length of the cell. These secondary effects become evident within a cell of finite length, but are not included within the coupled constitutive relationships, such as Eq. (57), which is applicable to a continuum element of infinitesimal length.

From Figs. 11(a) and 13(a), the cross-sectional rotation on either end of the cell in the two planes, as

$$\psi_z = \frac{2.6496 \times 10^{-9}}{H/3} = 2.6775 \times 10^{-8}, \ \psi_y = \frac{4.5892 \times 10^{-9}}{L/2} = 2.6775 \times 10^{-8}. \tag{51a, b}$$

Moreover, the y- and z-direction displacements within vectors $\mathbf{w}^*_{17}$ and $\mathbf{w}^*_{17R}$, and $\mathbf{w}^*_{18}$ and $\mathbf{w}^*_{18R}$ suggests a shift of the centre of area on the left-hand side of the cell for both, as shown in Figs. 15 and 16, respectively. The centre line slope rotations within the two shear vectors can then be determined as

$$\frac{\partial v}{\partial x} = \frac{7.1807 \times 10^{-10}}{0.3428} = 2.0947 \times 10^{-9}, \quad \frac{\partial w}{\partial x} = \frac{7.1807 \times 10^{-10}}{0.3428} = 2.0947 \times 10^{-9}, \tag{52a, b}$$

so the shear angles in the two planes are

$$\gamma_{xy} = \psi_z - \partial v/\partial x = 2.4680 \times 10^{-8}, \ \gamma_{xz} = \psi_y - \partial w/\partial x = 2.4680 \times 10^{-8}. \tag{53a, b}$$

From the above discussion on the bending moment vectors, it is known that a pure bending moment produces a bending curvature in the principal plane and a coupled shear deformation in the perpendicular plane. According to the reciprocal theorem, when the cell is subject to a shear, it should result in a shear deformation in the principal plane, coupled with a bending curvature in the perpendicular plane; from Figs. 12(a) and 14(a), these two coupled bending curvatures are, respectively

$$\frac{1}{R_z} = \frac{6.8056 \times 10^{-10}}{L/2 \times L/2} = 2.3166 \times 10^{-8} \text{ m}^{-1}, \quad \frac{1}{R_y} = \frac{3.9292 \times 10^{-10}}{H/3 \times L/2} = 2.3166 \times 10^{-8} \text{ m}^{-1}. \tag{54a, b}$$

The secondary bending curvatures produced by the bending moments M_z and M_y applied on the left-hand side of the cell, vectors $\mathbf{w}^*_{17}$ and $\mathbf{w}^*_{18}$, but regarded as being linearly distributed along the cell from the left-side to the right which, from Figs. 11(b) and 13(b), are

$$\frac{1}{R'_y} = \frac{7.2169 \times 10^{-10}}{H/3 \times L/2} = 4.2549 \times 10^{-8} \text{ m}^{-1}, \ \frac{1}{R'_z} = \frac{1.25 \times 10^{-9}}{L/2 \times L/2} = 4.2549 \times 10^{-8} \text{ m}^{-1}. \tag{55a, b}$$

From Figs. 12(b) and 14(b), the secondary coupled shear angles due to these bending moments in the perpendicular planes are

$$\gamma'_{xy} = \frac{5.2729 \times 10^{-9}}{L/2} = 3.0764 \times 10^{-9}, \quad \gamma'_{xz} = \frac{3.0443 \times 10^{-10}}{H/3} = 3.0764 \times 10^{-9}. \tag{56a, b}$$

As presaged above, the bending curvatures and shear angles obtained in Eqs. (55) and (56) are exactly one-half of those obtained in Eqs. (44) and (45), respectively.

The absence of bending–bending coupling for the example structure suggests that any proposed equivalent continuum coupling involving bending and shear will not be typical of a pre-twisted structure; indeed, the coupling appears to be closer to that of an asymmetric structure based upon a *NASA* deployable framework treated by Stephen and Zhang (2004), according to

$$\begin{bmatrix} Q_z \\ M_z \end{bmatrix} = \begin{bmatrix} \kappa_{xz} AG & K_{xz} \\ K_{xz} & EI_z \end{bmatrix} \begin{bmatrix} \gamma_{xz} \\ \partial \psi_z / \partial x \end{bmatrix}, \tag{57}$$

with an equivalent expression for bending in the perpendicular plane. In order to determine the equivalent second moment of area and shear coefficient, it is more convenient to write Eq. (57) in its inverted form

$$\begin{bmatrix} \gamma_{xz} \\ 1/R_y \end{bmatrix} = \mathbf{N} \begin{bmatrix} Q_z \\ M_z \end{bmatrix}. \tag{58}$$

where $\mathbf{N}$ is the compliance matrix

$$\mathbf{N} = \begin{bmatrix} n_{11} & n_{12} \\ n_{21} & n_{22} \end{bmatrix} = \begin{bmatrix} \kappa_{xz} AG & K_{xz} \\ K_{xz} & EI_z \end{bmatrix}^{-1}. \tag{59}$$

From the bending vector in the xy-plane, $\mathbf{w}_{15}$, one has $M_z = 9.9185 \times 10^{-3}$ Nm, $Q_z = 0$, $1/R_y = 8.5098 \times 10^{-8}\ \mathrm{m}^{-1}$, $\gamma_{xz} = 6.1527 \times 10^{-9}$, and substituting into Eq. (59) gives

$$n_{12} = \frac{\gamma_{xz}}{M_z} = 6.2033 \times 10^{-7},\ n_{22} = \frac{1/R_y}{M_z} = 8.5797 \times 10^{-6}. \tag{60a, b}$$

From the shear vector in the xz-plane $\mathbf{w}^*_{18}$, one has $M_z = 0$ Nm, $Q_z = 2.8934 \times 10^{-2}$ N, $1/R_y = 2.3166 \times 10^{-8}\ \mathrm{m}^{-1}$, $\gamma_{xz} = 2.4680 \times 10^{-8}$, and from Eq. (59)

$$n_{11} = \frac{\gamma_{xz}}{Q_z} = 8.5298 \times 10^{-7}, \quad n_{21} = \frac{1/R_y}{Q_z} = 8.0064 \times 10^{-7}. \tag{61a, b}$$

Inversion of the matrix N gives

$$\begin{bmatrix} \kappa_{xz} AG & K_{xz} \\ K_{xz} & EI_z \end{bmatrix} = \begin{bmatrix} n_{11} & n_{12} \\ n_{21} & n_{22} \end{bmatrix}^{-1} = \begin{bmatrix} 1.2577 \times 10^6 & -9.0935 \times 10^4 \\ -1.1737 \times 10^5 & 1.2504 \times 10^5 \end{bmatrix}, \tag{62}$$

from which the equivalent second moment of area is $I_z = 1.7863 \times\ 10^{-6}\ \mathrm{m}^4$, and shear coefficient $\kappa_{xz} = 0.4134$. However, Eqs. (60) and (61) indicate unequal coupling coefficients since $n_{12} \neq n_{21}$. Therefore, the coupled equations are modified, to read

$$\begin{bmatrix} Q_z \\ M_z \end{bmatrix} = \begin{bmatrix} \kappa_{xz} AG & K_{xz} \\ K_{zx} & EI_z \end{bmatrix} \begin{bmatrix} \gamma_{xz} \\ \partial \psi_z / \partial x \end{bmatrix}, \tag{63}$$

and the two coupling coefficients are $K_{xz} = -9.0935 \times 10^4$ Nm, $K_{zx} = -1.1737 \times 10^5$ Nm.

Similarly, from the bending vector in the xz-plane, $\mathbf{w}_{16}$, and the shear vector in the xy-plane, $\mathbf{w}^*_{17}$, it is found that $\kappa_{xy} = \kappa_{xz}$, $I_y = I_z$, $K_{xy} = K_{xz}$ and $K_{yx} = K_{zx}$, within the coupled equations

$$\begin{bmatrix} Q_y \\ M_y \end{bmatrix} = \begin{bmatrix} \kappa_{xy} AG & K_{xy} \\ K_{yx} & EI_y \end{bmatrix} \begin{bmatrix} \gamma_{xy} \\ \partial \psi_y / \partial x \end{bmatrix}; \tag{64}$$

equality of these properties was expected given the equilateral triangular cross-section of the example structure. However, the asymmetry of coupling within these stiffness matrices is contrary to the reciprocal theorem, and may imply that the coupled bending-shear model employed is inadequate for this particular structure, although other interpretations are possible. First, note that the cross-sectional displacements, that is, rotation and shear, are based on the three nodal axial displacements on both sides of the cell, and that it is always possible for a plane to pass through three given points; thus it is entirely possible, at least for this triangular cross-section, for a possible cross-sectional warping to be misinterpreted as a

rotation. This could be confirmed, or discounted, by the analysis of a pre-twisted structure having, say, a rectangular cross-section, and will be investigated in further work. Another possibility is a lack of work-conjugacy in relation to moments and rotations, which according to Ritto-Correa and Camotim (2003) is known to lead to asymmetric tangent matrices in large displacement, small strain analysis. It is also quite possible that the particular way of presenting the moment-shear coupling needs modification for a pre-twisted structure: thus when one calculates the nodal stiffness matrix **K**, in global coordinates, which is the first step of the analysis procedure, one is relating nodal force and displacement components *on both sides* of the cell. However, in writing constitutive relationships such as those expressed in Eq. (57), moment and shearing force are only explicitly stated for the left-hand side of the cell, consistent with an infinitesimal element, while those on the right-hand are understood; likewise, curvature and shear are interpreted from the rotation of the cross-section on both sides of the cell. For a straight structure this is quite acceptable—for example, moment equilibrium would require that there is an equal but opposite moment on the right-hand side, while cross-sectional rotations are always expressed within a global coordinate system. For the pre-twisted cell, the implied right-hand side moment is only equal and opposite within the global coordinate system, not the local. A further difficulty lies with the cross-sectional rotation, as finite rotations about different axes are known not to commute; this problem does not arise in the case of tension–torsion coupling, since the cross-sectional rotation (deformation) does commute with angle of pre-twist, as they are both about the same axis.

The inability to resolve this issue highlights the need for further research in the general area of bending of pre-twisted structures—both for the idealised discrete structure considered here, and for continuum rods, as in a pre-twisted turbine blade. However, one should emphasise that this issue represents a weakness in interpretation and current understanding, not an error in the principal vectors obtained by the eigenanalysis described in this paper—these must be correct, otherwise one would not obtain the correct Jordan canonical form.

6. Conclusions

Through introduction of a local coordinate system rotating with the cross-section—equivalent to the approach adopted in most, if not all, of the *Theory of Elasticity* approaches to the analysis of pre-twisted continuum beams or rods—the transfer matrix of each cell of a pre-twisted structure becomes identical; one then has translational symmetry, allowing eigenanalysis. Non-unity eigenvalues describe the rates of decay of self-equilibrated end loading, as anticipated by Saint-Venant's principle. Eigen- and principal vectors associated with the multiple real unity eigenvalues pertain to tension–torsion coupling, and equivalent continuum properties are determined; coupling is symmetric as one would expect from the reciprocal theorem. Interpretation of these vectors is simple, as a torsional deformation will commute with the angle of pre-twist. A variety of real and imaginary Jordan block forms are possible for the multiple complex unity eigenvalues, and these are discussed in some detail. Interpretation of the associated vectors is more difficult, even when presented in their simplest real forms; a pure bending moment produces a curvature in the plane of bending together with a shear in the perpendicular plane. In all likelihood, the choice of an example structure having equilateral triangular cross-section, and hence equal equivalent second moments of area, is responsible for the absence of bending–bending coupling; future extension of the approach to a rectangular cross-section should confirm such coupling, and would also allow investigation of cross-sectional warping. Interpretation of the shear vectors is the most difficult—a shearing force induces a linearly varying bending moment, cross-sectional rotations do not commute with the angle of pre-twist—and the asymmetry of coupling coefficients between bending and shear suggests that the model employed may be inadequate. On the other hand, asymmetric stiffness matrices are known to occur.

Appendix A. Transformation matrix and Jordan canonical form

$$\mathbf{V}=\begin{bmatrix}
-2.6441\times10^{-8} & -5.9282\times10^{-8} & -1.6709\times10^{-8} & -1.5171\times10^{-8} & 5.9694\times10^{-8} & -2.6441\times10^{-8}\\
-7.8780\times10^{-8} & -2.2359\times10^{-7} & -1.3240\times10^{-7} & 8.6401\times10^{-8} & 1.3240\times10^{-7} & 1.5472\times10^{-8}\\
-6.3349\times10^{-8} & -4.6575\times10^{-8} & 8.6401\times10^{-8} & 4.6575\times10^{-8} & -2.2359\times10^{-7} & 9.9900\times10^{-8}\\
-2.6441\times10^{-8} & 1.5171\times10^{-8} & 5.9694\times10^{-8} & 5.9282\times10^{-8} & -1.6709\times10^{-8} & -2.6441\times10^{-8}\\
-1.5472\times10^{-8} & 8.6410\times10^{-8} & -1.3240\times10^{-7} & -2.2359\times10^{-7} & 1.3240\times10^{-7} & 7.8782\times10^{-8}\\
9.9900\times10^{-8} & -4.6575\times10^{-8} & -2.2359\times10^{-7} & 4.6575\times10^{-8} & 8.6401\times10^{-8} & -6.3349\times10^{-8}\\
-2.6441\times10^{-8} & 4.4111\times10^{-8} & -4.2986\times10^{-8} & -4.4111\times10^{-8} & -4.2986\times10^{-8} & -2.6441\times10^{-8}\\
9.4252\times10^{-8} & -6.8595\times10^{-8} & 1.3606\times10^{-7} & -6.8595\times10^{-8} & -1.3606\times10^{-7} & -9.4252\times10^{-8}\\
-3.6650\times10^{-8} & 2.2189\times10^{-7} & -6.8595\times10^{-8} & -2.2189\times10^{-7} & -6.8595\times10^{-8} & -3.6550\times10^{-8}\\
0 & 0 & 0 & 0 & 0 & 0\\
-1/2 & -\sqrt{3}/2 & -1/2 & -\sqrt{3}/2 & -1/2 & -1/2\\
-\sqrt{3}/2 & -1/2 & \sqrt{3}/2 & -1/2 & \sqrt{3}/2 & -\sqrt{3}/2\\
0 & 0 & 0 & 0 & 0 & 0\\
-1/2 & \sqrt{3}/2 & -1/2 & \sqrt{3}/2 & -1/2 & -1/2\\
\sqrt{3}/2 & -1/2 & -\sqrt{3}/2 & -1/2 & -\sqrt{3}/2 & \sqrt{3}/2\\
0 & 0 & 0 & 0 & 0 & 0\\
1 & 0 & 1 & 0 & 1 & 1\\
0 & 1 & 0 & 1 & 0 & 0\\
1\times10^{-8} & 0 & 0 & 0 & 0 & 0\\
0 & 8.4417\times10^{-10} & 8.57\times10^{-8} & 3.8019\times10^{-11} & 1\times10^{-8} & 0\\
0 & 1.4621\times10^{-9} & -4.9479\times10^{-8} & 6.5851\times10^{-11} & 0 & 1\times10^{-8}\\
1\times10^{-8} & 0 & 0 & 0 & 0 & 0\\
0 & 8.4417\times10^{-10} & -8.57\times10^{-8} & 3.8019\times10^{-11} & 1\times10^{-8} & 0\\
0 & -1.4621\times10^{-9} & -4.9479\times10^{-8} & -6.5851\times10^{-11} & 0 & 1\times10^{-8}\\
1\times10^{-8} & 0 & 0 & 0 & 0 & 0\\
0 & -1.6883\times10^{-9} & 0 & -7.6039\times10^{-11} & 1\times10^{-8} & 0\\
0 & 0 & 9.8958\times10^{-8} & 0 & 0 & 1\times10^{-8}\\
0 & 7.6469\times10^{-2} & 0 & -9.0323\times10^{-3} & 0 & 0\\
0 & -7.9046\times10^{-3} & 0 & 7.4604\times10^{-3} & 0 & 0\\
0 & 4.5637\times10^{-3} & 0 & -4.3073\times10^{-3} & 0 & 0\\
0 & 7.6469\times10^{-2} & 0 & -9.0323\times10^{-3} & 0 & 0\\
0 & 7.9046\times10^{-3} & 0 & -7.4604\times10^{-3} & 0 & 0\\
0 & 4.5637\times10^{-3} & 0 & -4.3073\times10^{-3} & 0 & 0\\
0 & 7.6469\times10^{-2} & 0 & -9.0323\times10^{-3} & 0 & 0\\
0 & 0 & 0 & 0 & 0 & 0\\
0 & -9.1274\times10^{-3} & 0 & 8.6146\times10^{-3} & 0 & 0\\
2.8868\times10^{-9} & 5\times10^{-9} & -3.8880\times10^{-10} & -3.1089\times10^{-9} & 2.0225\times10^{-9} & 5.9385\times10^{-9}\\
0 & 0 & 3.5904\times10^{-10} & 6.2187\times10^{-10} & -6.3152\times10^{-10} & -4.6455\times10^{-10}\\
0 & 0 & 6.2187\times10^{-10} & 1.0771\times10^{-9} & -1.0938\times10^{-9} & -8.0462\times10^{-10}\\
2.8868\times10^{-9} & -5\times10^{-9} & -2.4980\times10^{-9} & 1.8911\times10^{-9} & 4.1317\times10^{-9} & -4.7208\times10^{-9}\\
0 & 0 & 3.5904\times10^{-10} & -6.2187\times10^{-10} & -8.6547\times10^{-11} & 7.7919\times10^{-10}\\
0 & 0 & -6.2187\times10^{-10} & 1.0771\times10^{-9} & 1.4990\times10^{-10} & -1.3496\times10^{-9}\\
-5.7735\times10^{-9} & 0 & 2.8868\times10^{-9} & 1.2177\times10^{-9} & -6.1542\times10^{-9} & -1.2177\times10^{-9}\\
0 & 0 & 1.4361\times10^{-9} & 0 & -1.4361\times10^{-9} & 6.2928\times10^{-10}\\
0 & 0 & 0 & 0 & 0 & 0\\
0 & 0 & 1.6705\times10^{-2} & 2.8934\times10^{-2} & -2.7259\times10^{-3} & -3.7005\times10^{-2}\\
0 & 0 & -3.5656\times10^{-3} & -2.0586\times10^{-3} & -5.9174\times10^{-3} & 1.7786\times10^{-3}\\
0 & 0 & -2.0586\times10^{-3} & 3.5656\times10^{-3} & 1.7787\times10^{-3} & -1.3372\times10^{-2}\\
0 & 0 & 1.6705\times10^{-2} & -2.8934\times10^{-2} & -3.0684\times10^{-2} & 2.0863\times10^{-2}\\
0 & 0 & 3.5656\times10^{-3} & -2.0586\times10^{-3} & -1.3049\times10^{-2} & 2.3385\times10^{-3}\\
0 & 0 & -2.0586\times10^{-3} & -3.5656\times10^{-3} & 2.3385\times10^{-3} & -6.2406\times10^{-3}\\
0 & 0 & -3.3410\times10^{-2} & 0 & 3.3410\times10^{-2} & 1.6142\times10^{-2}\\
0 & 0 & 0 & 4.1142\times10^{-3} & -9.9678\times10^{-3} & -4.1172\times10^{-3}\\
0 & 0 & 4.1172\times10^{-3} & 0 & -4.1172\times10^{-3} & -9.3213\times10^{-3}
\end{bmatrix},$$

$\mathbf{V}^{-1}\mathbf{G}'\mathbf{V} = \mathbf{J}$, where $\mathbf{J}$ is the real Jordan block matrix.

$$\mathbf{J} = \begin{bmatrix}
-22.3303 & 0 & 0 & 0 & 0 & 0 & 0 & 0 & 0 & 0 & 0 & 0 & 0 & 0 & 0 & 0 & 0 & 0 \\
0 & -10.0110 & -10.0110 & 0 & 0 & 0 & 0 & 0 & 0 & 0 & 0 & 0 & 0 & 0 & 0 & 0 & 0 & 0 \\
0 & 10.0110 & -10.0110 & 0 & 0 & 0 & 0 & 0 & 0 & 0 & 0 & 0 & 0 & 0 & 0 & 0 & 0 & 0 \\
0 & 0 & 0 & -0.0499 & -0.0499 & 0 & 0 & 0 & 0 & 0 & 0 & 0 & 0 & 0 & 0 & 0 & 0 & 0 \\
0 & 0 & 0 & 0.0499 & -0.0499 & 0 & 0 & 0 & 0 & 0 & 0 & 0 & 0 & 0 & 0 & 0 & 0 & 0 \\
0 & 0 & 0 & 0 & 0 & -0.0448 & 0 & 0 & 0 & 0 & 0 & 0 & 0 & 0 & 0 & 0 & 0 & 0 \\
0 & 0 & 0 & 0 & 0 & 0 & 1 & 1 & 0 & 0 & 0 & 0 & 0 & 0 & 0 & 0 & 0 & 0 \\
0 & 0 & 0 & 0 & 0 & 0 & 0 & 1 & 0 & 0 & 0 & 0 & 0 & 0 & 0 & 0 & 0 & 0 \\
0 & 0 & 0 & 0 & 0 & 0 & 0 & 0 & 1 & 1 & 0 & 0 & 0 & 0 & 0 & 0 & 0 & 0 \\
0 & 0 & 0 & 0 & 0 & 0 & 0 & 0 & 0 & 1 & 0 & 0 & 0 & 0 & 0 & 0 & 0 & 0 \\
0 & 0 & 0 & 0 & 0 & 0 & 0 & 0 & 0 & 0 & c & -s & c & -s & 0 & 0 & 0 & 0 \\
0 & 0 & 0 & 0 & 0 & 0 & 0 & 0 & 0 & 0 & s & c & s & c & 0 & 0 & 0 & 0 \\
0 & 0 & 0 & 0 & 0 & 0 & 0 & 0 & 0 & 0 & 0 & 0 & c & -s & c & -s & 0 & 0 \\
0 & 0 & 0 & 0 & 0 & 0 & 0 & 0 & 0 & 0 & 0 & 0 & s & c & s & c & 0 & 0 \\
0 & 0 & 0 & 0 & 0 & 0 & 0 & 0 & 0 & 0 & 0 & 0 & 0 & 0 & c & -s & c & -s \\
0 & 0 & 0 & 0 & 0 & 0 & 0 & 0 & 0 & 0 & 0 & 0 & 0 & 0 & s & c & s & c \\
0 & 0 & 0 & 0 & 0 & 0 & 0 & 0 & 0 & 0 & 0 & 0 & 0 & 0 & 0 & 0 & c & -s \\
0 & 0 & 0 & 0 & 0 & 0 & 0 & 0 & 0 & 0 & 0 & 0 & 0 & 0 & 0 & 0 & s & c
\end{bmatrix},$$

where $c = \cos\alpha$, $s = \sin\alpha$ and $\alpha = \pi/8$.

Appendix B. Two shear vectors

$$[\,\mathbf{w}_{17}^{*} \quad \mathbf{w}_{18}^{*}\,] = \begin{bmatrix}
3.5245 \times 10^{-9} & 5.7507 \times 10^{-9} \\
-9.3197 \times 10^{-10} & -2.9108 \times 10^{-10} \\
-1.6142 \times 10^{-9} & -5.0417 \times 10^{-10} \\
3.2180 \times 10^{-9} & -5.9277 \times 10^{-9} \\
2.1390 \times 10^{-10} & 9.5265 \times 10^{-10} \\
-3.7049 \times 10^{-10} & -1.6500 \times 10^{-9} \\
-6.7425 \times 10^{-9} & 1.7698 \times 10^{-9} \\
-1.4361 \times 10^{-9} & 1.3231 \times 10^{-10} \\
0 & 0 \\
-1.6705 \times 10^{-3} & -2.8934 \times 10^{-2} \\
-4.9228 \times 10^{-3} & 5.5975 \times 10^{-5} \\
5.5975 \times 10^{-5} & -1.4366 \times 10^{-2} \\
-1.6705 \times 10^{-2} & 2.8934 \times 10^{-2} \\
-1.2054 \times 10^{-2} & 4.0612 \times 10^{-3} \\
4.0612 \times 10^{-3} & -7.2352 \times 10^{-3} \\
3.3410 \times 10^{-2} & 0 \\
-1.1957 \times 10^{-2} & -4.1172 \times 10^{-3} \\
-4.1172 \times 10^{-3} & -7.3322 \times 10^{-3}
\end{bmatrix}$$

References

Chen, C., 1951. The effect of initial twist on the torsional rigidity of thin prismatical bars and tubular members. In: Proceedings of the First US National Congress of Applied Mechanics. ASME, New York.

Di Prima, R.C., 1959. Coupled torsional and longitudinal vibrations of a thin bar. ASME Journal of Applied Mechanics 26 (4), 510–512.

Goodier, J.N., Griffin, D.S., 1969. Elastic bending of pretwisted bars. International Journal of Solids and Structures 5 (11), 1231–1245.

Guglielmino, E., Saccomandi, G., 1996. On the bending of pretwisted bars by a terminal transverse load. International Journal of Engineering Science 34 (11), 1285–1299.

Kelley, W.G., Peterson, A.C., 2001. Difference equations, second ed. Academic Press, New York.

Krenk, S., 1983a. A linear theory for pretwisted elastic beams. ASME Journal of Applied Mechanics 50 (1), 137–142.

Krenk, S., 1983b. The torsion-extension coupling in pretwisted elastic beams. International Journal of Solids and Structures 19 (1), 67–72.

Okubo, H., 1951. The torsion and stretching of spiral rods (I). Quarterly of Applied Mathematics 9 (3), 263–272.

Okubo, H., 1953. The torsion of spiral rods. ASME Journal of Applied Mechanics 20 (2), 273–278.

Okubo, H., 1954. The torsion and stretching of spiral rods (II). Quarterly of Applied Mathematics 11 (4), 488–495.

Pucci, E., Risitano, A., 1996. Bending of a pretwisted bar by terminal transverse load. International Journal of Engineering Science 34 (4), 437–452.

Ritto-Correa, M., Camotim, D., 2003. Work-conjugacy between rotation dependent moments and finite rotations. International Journal of Solids and Structures 40 (11), 2851–2873.

Rosen, A., 1991. Structural and dynamic behaviour of pretwisted rods and beams. ASME Applied Mechanics Reviews 44 (12), 483–515.

Shield, R.T., 1982. Extension and torsion of elastic bars with initial twists. ASME Journal of Applied Mechanics 49 (4), 779–786.

Stephen, N.G., Wang, P.J., 1996. On Saint-Venant's principle in pin-jointed frameworks. International Journal of Solids and Structures 33 (1), 79–97.

Stephen, N.G., Zhang, Y., 2004. Eigenanalysis and continuum modelling of an asymmetric beam-like repetitive structure. International Journal of Mechanical Sciences 46 (8), 1213–1231.

Tabarrok, B., Xiong, Y., 1989. On the buckling equations for spatial rods. International Journal of Mechanical Sciences 31 (3), 179–192.